Spring 2020

Monitoring and Identifying the Rhodamine 6G-Hydroxide Ion Reaction Using In-Situ, Surface-Enhanced Raman Spectroscopy

Ryan Lamb
Western Kentucky University, ryan.lamb983@topper.wku.edu

MONITORING AND IDENTIFYING THE RHODAMINE 6G-HYDROXIDE ION REACTION USING IN-SITU, SURFACE-ENHANCED RAMAN SPECTROSCOPY

A Thesis
Presented to
The Faculty of the Department of Chemistry
Western Kentucky University
Bowling Green, Kentucky

In Partial Fulfillment
Of the Requirements of the Degree
Master of Science

By
Ryan M. Lamb

May 2020

MONITORING AND IDENTIFYING THE RHODAMINE 6G-HYDROXIDE ION REACTION USING IN-SITU, SURFACE-ENHANCED RAMAN SPECTROSCOPY

Date Recommended 3/20/2020

Matthew Nee Digitally signed by Matthew Nee Date: 2020.04.13 16:31:11 -05'00'

Dr. Matthew Nee, Director of Thesis

Eric Conte Digitally signed by Eric Conte Date: 2020.04.13 17:57:49 -05'00'

Dr. Eric Conte

Bangbo Yan Digitally signed by Bangbo Yan Date: 2020.04.13 19:30:44 -05'00'

Dr. Bangbo Yan

Cheryl D Davis Digitally signed by Cheryl D Davis Date: 2020.04.15 12:44:42 -05'00'

Dean, Graduate School Date

I dedicate this thesis to my mom, Christie Lamb, who has done so much for me.

ACKNOWLEDGEMENTS

I would first like to thank my research advisor, Dr. Matthew Nee, who has mentored me through 4 years of research. He has taught me so much and has made this research experience very enjoyable. I feel like I am well prepared for the next step in my academic career, and it is all thanks to him. I would also like to thank my former and current research group members for their support: Frankie Wallace, J.R. Bertram, Konnor Jones, Jesus Berlanga, Kayla Steward, Maxwell Conte, Lovence Ainembabazi, Matthew Broadbent, Paul Portmann, Megan Hesse, and Connor Schulte. I would also like to recognize Dr. John Andersland for his help with using the TEM. Thank you to my close friends and family for supporting and encouraging me throughout this experience.

Funding for this project was provided by WKU Faculty-Undergraduate Student Engagement (FUSE), the Kentucky Academy of Science (KAS), and Research & Creative Activities Program (RCAP).

TABLE OF CONTENTS

LIST OF FIGURES

Figure Page

LIST OF CHARTS

LIST OF SCHEMES

MONITORING AND IDENTIFYING THE RHODAMINE 6G-HYDROXIDE ION REACTION USING IN-SITU, SURFACE-ENHANCED RAMAN SPECTROSCOPY

Ryan Lamb May 2020 48 Pages

Directed by: Dr. Matthew Nee, Dr. Eric Conte, and Dr. Bangbo Yan

Department of Chemistry Western Kentucky University

An effective method for monitoring chemical reactions is necessary to better understand their mechanisms and kinetics. Effective reaction monitoring requires a spectroscopy technique with fast data acquisition, high sensitivity, structure-to-spectrum correlation, and low solvent interference. Surface-enhanced Raman spectroscopy (SERS) provides these features, which makes it a valuable tool for monitoring reactions. To obtain the Raman enhancement, metallic nanostructures typically made of silver or gold are aggregated using a salt. The nanoparticles aggregates must then be stabilized using a surfactant to use this method *in situ* due to eventual nanoparticle precipitation. In this study, gold nanoparticles stabilized with sodium dodecyl sulfate (SDS) were used to monitor an aqueous reaction involving rhodamine 6G (R6G) and hydroxide ion. Through a series of experiments, the most probable reaction mechanism for this reaction was determined from three predicted mechanisms: saponification, dimerization, and deprotonation. The deprotonation mechanism resulted in the most supporting evidence, and the saponification and dimerization mechanisms were rejected as probable reaction mechanisms.

CHAPTER 1

Finding an Innovative Reaction Monitoring Method

Finding an effective method for monitoring reactions has been a growing area of research in chemistry that has significance in both industrial and academic frameworks. Reaction monitoring is the process of tracking the consumption of reactants or the production of products in order to determine information about a particular reaction, such as its mechanisms or kinetics. It is often used in manufacturing processes to ensure desired products are being produced.[1] In academia, research involving reaction monitoring often focuses on studying reactions that are not yet well understood. Such reactions usually have potentially significant applications in the real world (e.g. photodegradation of organic wastewater pollutants, solar energy harvesting, carbon dioxide capturing, etc.).

1.1 Common Reaction Monitoring Methods

An ideal reaction monitoring technique would have fast data acquisition, high sensitivity, structure-to-spectrum correlation, and low solvent interference. Fast data acquisition would allow the reaction monitoring method to monitor fast reactions (such as reactions that reach equilibrium in less than a minute), since the rate of data collection would need to be faster than the rate of a reaction to effectively monitor it. Furthermore, high sensitivity means that a large response is observed without the need of a large amount of analyte (e.g. a high concentration). High sensitivity is particularly important for obtaining a high signal-to-noise ratio and conserving materials (by using less analyte to achieve adequate signal). Structure-to-spectrum correlation means that the data collected from a given reaction monitoring method can be connected to the molecular structure of the analyte. Structure-to-spectrum correlation is important because changes in the spectra

over the course of a reaction can be used to determine the changes in the molecular structure during said reaction, leading to more accurate reaction mechanisms. Lastly, low solvent interference means the signal due to the solvent of a given analyte is small compared to the signal of the analyte. Low solvent interference helps with improving the signal-to-noise ratio.

1.1.1 Chromatography-Mass Spectrometry

A possible way to monitor reactions is to use chromatography-mass spectrometry.[2] Chromatography is an analytical technique used to separate components of a mixture that can exist in the gas phase (GC) or liquid phase (LC). Mass spectrometry (MS) is an analytical technique that involves ionizing chemical species and sorting the ions based on their mass-to-charge ratio. Together, these techniques can be used to separate and accurately identify components of a mixture. Although this method can provide a substantial amount of information about the intermediates of the reaction, it is a relatively slow process (often taking minutes to collect one chromatogram),[2] thus being ineffective for detection of short-lived intermediates (e.g. intermediates with a lifespan of less than a few minutes) and determination of the kinetics of a reaction. Chromatography-mass spectrometry often requires extensive sample preparation, such as extraction of analyte from a sample matrix or pre-concentration/dilution of analyte. These sample preparation procedures are meant to reduce interference from the sample matrix and improve the signal-to-noise ratio of the analyte. Due to the slow data acquisition and extensive sample prep required, chromatography-mass spectrometry is not an ideal reaction monitoring method for fast reactions or complex samples.

1.1.2 Nuclear Magnetic Resonance (NMR) Spectroscopy

Nuclear magnetic resonance spectroscopy involves applying a strong magnetic field to a sample and then probing with electromagnetic radiation (in the radio wave region) to get information about the chemical environments of the nuclei present in the sample.[3] By applying a magnetic field to a sample, two different spin states are created: the α-spin state, which is aligned with the external magnetic field and lower in energy, and the β-spin state, which is aligned against the external magnetic field and higher in energy. Nuclei can be excited from the α-spin state to the β-spin state via radio waves. The energy gap between these states is related to the amount of electron shielding of each nucleus. Therefore, each unique chemical environment will have a different amount of energy between the α-spin state to the β-spin state, which will each produce a distinct signal in NMR. The most common types of NMR spectroscopy are proton-NMR (^{1}H-NMR) and carbon-NMR (^{13}C-NMR), which deliver information about the chemical environments of hydrogen atoms and carbon atoms in samples, respectively. By tracking the signals in an NMR spectrum over the course of a reaction, a reaction can be monitored.[4] NMR spectroscopy offers suitable time resolution[5] (as fast as a few nanoseconds between samples), high sensitivity, and excellent structure-to-spectrum correlation. However, interference from the sample matrix can make interpreting the NMR spectra difficult. Additionally, the cost of acquiring and maintaining instruments sophisticated enough for effective reaction monitoring can be very great. Due to sample interference, NMR spectroscopy is not an ideal reaction monitoring method for complex samples.

1.1.3 Ultraviolet (UV)-Visible Absorption Spectroscopy

Ultraviolet (UV)-visible absorption is another possible strategy used to monitor reactions.[6] UV-visible absorption spectroscopy involves measuring the absorbance of an analyte either at a singular wavelength or for a range of wavelengths. The measured absorbance represents the excitation of molecules from ground state to an excited energy level. This method offers faster data acquisition than chromatographic techniques based on how fast the spectrometer can record an absorption spectrum.[6] In recent years, some spectrometers have been manufactured with a "kinetics" feature that tracks the absorbance value at a particular wavelength over time. This makes monitoring reactions particularly easy and simple. Since many common solvents do not absorb in the UV or visible range (such as water and methanol), there is often minimal interference from solvents. However, UV-visible absorption spectroscopy can only be used to monitor chemical species that absorb in the UV or visible range (such as metal complexes or conjugated organic molecules). Since absorbing at a given wavelength cannot be connected to a specific structural motif, UV-visible absorption spectroscopy does not provide much information (if any) about the molecular structure of the analyte or about the presence of intermediates. For example, Figure 1.1 shows the visible absorbance spectrum (from 400-650 nm) of aqueous $[Co(H_2O)_6]^{2+}$, aqueous rhodamine 6G, and 30-nm gold nanoparticle colloid. All three samples have a maximum

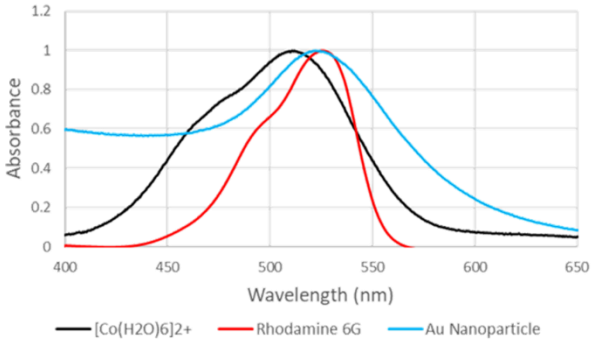

Figure 1.1. Visible absorbance spectra from 400-650 nm of aqueous $[Co(H_2O)_6]^{2+}$, aqueous rhodamine 6G, and 30-nm gold nanoparticle colloid.

absorbance between 510-525 nm despite having very different structures (i.e. a transition metal complex, a conjugated organic dye, and metal nanoparticles). In other words, there is no clear connection between the spectra and the molecular structure(s) involved in the reaction, which makes reaction mechanism determination difficult, if not impossible. Because UV-visible spectroscopy lacks structure-to-spectrum correlation, this method is not suitable for reaction monitoring with the purpose of determining reaction mechanisms but can be useful for determining the kinetics of specific reaction systems (i.e. analytes that absorb in the UV-visible range).

1.1.4 Fourier Transform-Infrared (FTIR) Spectroscopy

Fourier transform-infrared (FTIR) spectroscopy can also be used to monitor reactions.[7,8] In FTIR absorbed infrared radiation (relative absorbance) is measured from a solution as a function of photon wavenumbers (cm^{-1}). Absorbance of infrared radiation corresponds to excitation of the analyte to a higher energy vibrational state. Since IR absorption relates to molecular vibrations, changes in the IR spectrum can be connected to changes in the molecular structure. For example, as a certain bond breaks in solution, the absorption peak associated with that molecular vibration will decrease, and as a bond forms in solution, the absorption peak associated with that molecular vibration will increase. FTIR spectroscopy can have a time resolution as fast as a femtosecond;[9] however, the standard data collection rate is about 2 spectra per second.[8] This means FTIR can be used to determine the reaction kinetics and identify possible intermediates. However, monitoring aqueous reactions with FTIR spectroscopy can be problematic due to the broad, intense peaks that arise from the IR spectrum of water (Figure 1.2). For this reason, FTIR spectroscopy is not ideal for monitoring aqueous reactions.

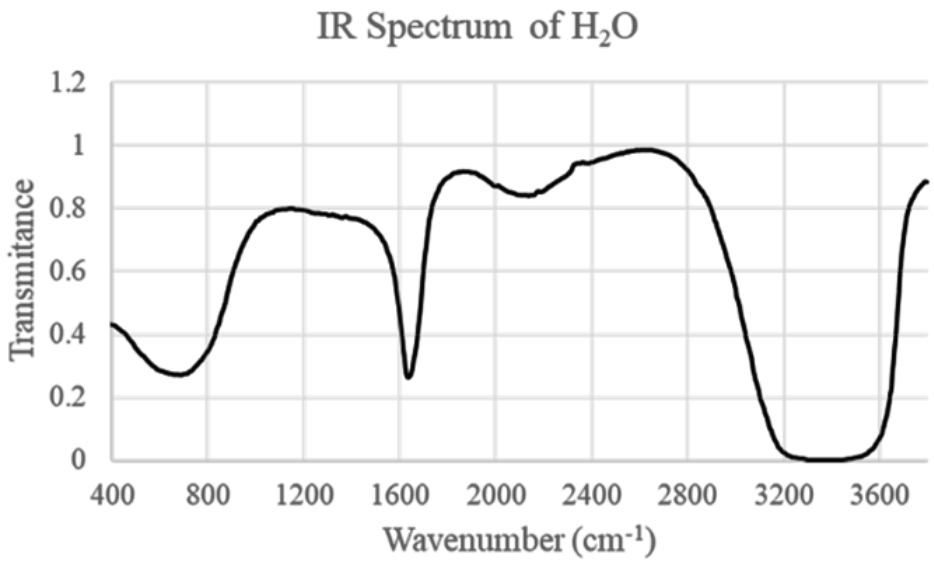

Figure 1.2. FTIR spectrum of water (H_2O). Data from Ref. 10.

1.2 Raman Spectroscopy

Raman scattering is the phenomenon in which a molecule redirects a photon in any direction. When the photon is scattered, it can either have the same energy as the incident photon or different energy. If the scattered photon has the same energy, the scattering is considered to be elastic and is termed Raleigh scattering. Raman scattering is inelastic because the scattered photon has a different energy than the incident photon. The scattering is called Stokes scattering if the scattered photon has less energy than the incident photon and anti-Stokes scattering if the scattered photon has more energy (Figure 1.3a). Since the change in energy (termed Raman shift) is equal to the vibrational energy levels of the molecule, plotting Raman intensity versus Raman shift (in cm^{-1}) will result in a spectrum where each peak is related to a vibrational mode of the molecule. Raman shift is calculated by subtracting the wavenumber (equivalent to 1/wavelength, thus making wavenumber proportional to energy) of the scattered photon from the wavenumber of the incident photon. Based on this calculation, Stokes scattering has a positive Raman shift, and anti-

Stokes has a negative Raman shift. Graphing Stokes and anti-Stokes scattering together yields mirror image spectra with peak centers at the same Raman shifts, but the anti-Stokes side of the spectrum will have significantly less intensity (Figure 1.3b). This decreased intensity is because the molecule has to already be in an excited vibrational state before encountering the incident photon, which is less likely than the molecule being in its ground vibrational state. Because there are more molecules in excited vibrational states as temperature increases, at higher temperatures the ratio of Anti-Stokes intensity to Stokes intensity approaches 1.[11,12] Stokes and Anti-Stokes scattering provide the same chemical

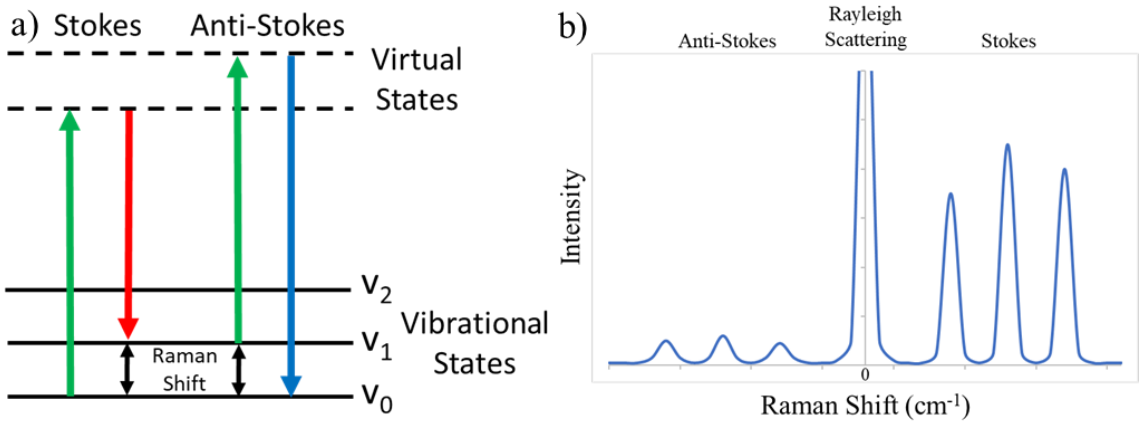

Figure 1.3. a) An energy diagram comparing stokes and anti-stokes scattering. An incident photon excites the molecule to a virtual state, indicated by the first green line. The photon can then be scattered with less energy than in started with (red line; Stokes scattering). Anti-Stokes scattering requires the molecule to be in an excited vibrational state before the scattering occurs (second green line). After scattering, the scattered photon can have more energy than the incident photon and the molecule will be in its ground state (blue line). b) The Raman spectrum of a theoretical molecule. A Raman spectrum consists of plotting Raman intensity vs Raman shift, which is calculated by subtracting the frequency of the scattered photon from the frequency of the incident photon. Based on this calculation, Raleigh scattering has a Raman shift of zero, Stokes scattering has a positive Raman shift, and Anti-Stokes has a negative Raman shift.

information (because they have identical Raman shifts), but due to the low intensity of Anti-Stokes scattering, most Raman spectra will only show the Stokes side of the spectrum.

Raman spectroscopy offers time resolution similar to FTIR spectroscopy. That is, Raman spectroscopy is capable of having femtosecond resolution and most commercial instruments can generate multiple Raman spectra per second. Raman spectroscopy also offers similar chemical information as FTIR spectroscopy. In other words, each Raman peak corresponds to a certain molecular vibration; therefore, changes in the Raman spectrum of an analyte can be related to changes in the molecular structure of said analyte. These features, fast data acquisition and structure-to-spectrum connection, make Raman spectroscopy ideal for monitoring reactions. Raman spectroscopy can even be used to monitor aqueous reactions due to the relatively small Raman cross section of water. This is because Raman scattering is dependent on the polarizability of a molecule. However, Raman spectroscopy has a drawback: Raman scattering occurs about one millionth as often as Raleigh scattering, which is already a weak occurrence.[13] This means that Raman intensity is usually negligibly small for low analyte concentrations (i.e. 10^{-6} M), making it difficult to monitor reactions.

1.3 Surface-Enhanced Raman Spectroscopy

Fortunately, Raman scattering can be enhanced by using surface-enhanced Raman spectroscopy (SERS). SERS involves the use of nanostructures made of precious metals (i.e. Ag or Au) to attain Raman enhancement.[14] These nanostructures can be in the form of nanoparticles, nanoclusters, nanoshells, and nanostars. Adsorbing an analyte molecule onto gold nanostructures has been shown to produce Raman enhancement factors of at least 10^6.[15,16] There are two proposed mechanisms responsible for this enhancement: an

electromagnetic mechanism and a chemical mechanism.[14] The electromagnetic mechanism involves the excitation of the nanostructure's plasmon. A plasmon is the collective oscillation of the conduction electrons of a nanostructure in response to electromagnetic radiation of the appropriate wavelength, typically in the visible or infrared range (Figure 1.4).[17] The resonant oscillation of the nanostructure's surface electrons (termed localized surface plasmon resonance) increases the electric field experienced by any molecules adsorbed to the nanoparticle's surface.[18] Since Raman intensity is dependent on the applied electric field, greatly increasing the electric field experienced by a molecule greatly increases its Raman intensity. The chemical mechanism involves charge-transfer between the nanostructure and the chemically bound analyte.[19] Essentially, the metal nanostructure plasmon is excited by a photon to a virtual state analogous to the virtual state of the analyte. The energy is then transferred to the analyte, which results in an excitation to a virtual state. The analyte relaxes and transfers the energy back to the nanostructure minus the vibrational energy of the analyte. The nanostructure then emits a photon with different energy than the incident photon (corresponding to a Stokes Raman shift). Theoretical calculations for non-aggregated nanoparticles estimated the Raman enhancement due to the electromagnetic mechanism to be at least 10^6, whereas the Raman enhancement due

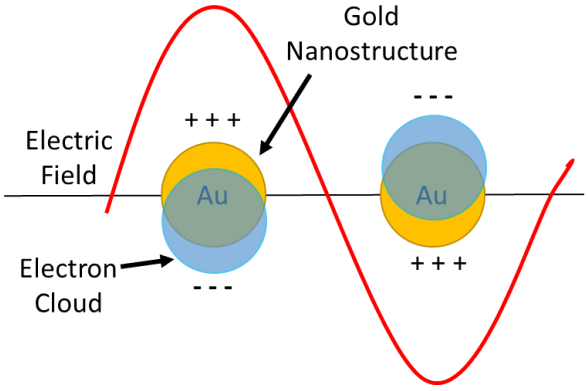

Figure 1.4. The presence of an electric field polarizes the nanostructures, making the surface electrons oscillate (called a plasmon). The generation of the localized surface plasmon resonance polarizes molecules adsorbed onto the surface of the nanostructure, leading to Raman enhancement.

to the chemical mechanism is estimated to be less than 10^2.[16] Additionally, theoretical calculations for nanoparticle dimers estimated a total Raman enhancement factor of at least 10^{11}. Since SERS offers identical chemical information as Raman spectroscopy, but with greater sensitivity, SERS can be used to monitor aqueous reactions as well.

SERS has already been used to monitor a few aqueous reactions in the literature in a variety of approaches.[20–22] A common trend in these approaches is to create bifunctional SERS nanostructures that can act simultaneously as a catalyst and a SERS-active substrate.[20] There has also been a focus on synthesizing magnetic SERS-active nanostructures to easily collect and re-use nanostructures at a later date.[21] Although these methods can be quite successful, they often involve meticulous synthetic procedures that can be costly in both time and money.

One of the main challenges of working with SERS nanostructures is long-term stability. Typically, to achieve effective Raman enhancement, nanoparticles need to be aggregated to form "hot spots" between neighboring nanoparticles, and analytes need to be located in said hot spots. The formation of these hot spots results in an inhomogeneous electric field in solution (discussed more in Section 2.2). Unfortunately, nanoparticle aggregation ultimately leads to precipitation of the nanoparticles and overall loss of Raman signal over time. There have been two approaches to alleviate this problem: (1) immobilizing the nanostructures on an inert surface[22] and (2) using a surfactant.[23] Overwhelmingly, immobilization seems to be the desired route for nanoparticle stabilization; however, this method has difficulties when it comes to heterogenous reactions and reactions which the reaction mixture cannot pass over the SERS substrate.

1.4 Nanoparticle Size and the "Particle-in-a-Box" Model

For a given nanoparticle colloid, the wavelength at which the maximum absorbance is located represents the energy needed to excite the plasmon of the nanoparticles in that colloid. The excitation energy of the plasmon of a nanoparticle is related to the size of the nanoparticle, which can be demonstrated using the particle-in-a-box model in quantum mechanics. The particle-in-a-box model is used to describe the energy states of a particle that is confined to a "box." The particle (in this case, an electron) can move freely within the box (i.e. the nanoparticle) because the potential energy is zero within the box, and the particle cannot leave the box because the potential energy is infinite outside the box. A nanoparticle is best represented by a three-dimensional box; however, a one-dimensional box can still be used to demonstrate a relationship between energy and size of the box. Solving the Schrodinger equation using this model yields:

$$E_n = \frac{n^2 h^2}{8mL^2} \tag{1}$$

Where E_n is the energy associated with a given energy state (n), h is Planck's constant (6.6×10^{-34} Js), m is the mass of the particle (electron) in kilograms, and L is the length of the one-dimensional box. According to Equation 1, the length (size) of the box is inversely proportional to the excitation energy of the nanoparticle which is inversely proportional to wavelength. Therefore, the size of the nanoparticle is directly proportional to the wavelength of maximum absorbance. That is, larger nanoparticles absorb at longer wavelengths (i.e. lower energy plasmon), and smaller nanoparticles absorb at shorter wavelengths (i.e. higher energy plasmon). In this way, the UV-visible spectrum of a nanoparticle colloid can be used to estimate the size and distribution of the nanoparticles in the colloid. The size and distribution of gold nanoparticles is particularly important,

since gold nanoparticles exhibit catalytic properties with diameters <10 nm and exhibit SERS properties with diameters >20 nm.[24]

1.5 Project Goals: Monitoring and Identification of Rhodamine 6G-Hydroxide Ion Reaction

Rhodamine 6G (R6G) is often used as a model analyte for photocatalytic[25–29] and SERS[30–32] studies. The use of R6G for photocatalytic studies is likely due to its connection to water pollution, and the use of R6G for SERS studies is likely due to its effectiveness at adsorbing onto SERS substrates. At the beginning of this research project, the photolysis of R6G was the reaction to be studied due to its applications in wastewater treatment, but the reaction between R6G and OH^- became the main focus of this research project after discovering that it is seemingly absent from the literature. The aim of this project is to effectively monitor the kinetics and determine the order of this reaction, along with identify possible reaction mechanisms for said reaction. Determination of the kinetics will be done by tracking changes in the Raman spectra over time. Identification of the reaction and its mechanisms will be done through a process-of-elimination approach due to the lack of information present in the literature. To aid in the reaction elimination process, supplementary compounds, rhodamine B (RB) and rhodamine 110 (R110), will be tested alongside R6G and the results will be compared. All three structures are shown in Chart 1.1. RB and R110 are used due to strategic differences in their structures relative to R6G, which Chart 1.1 emphasizes.

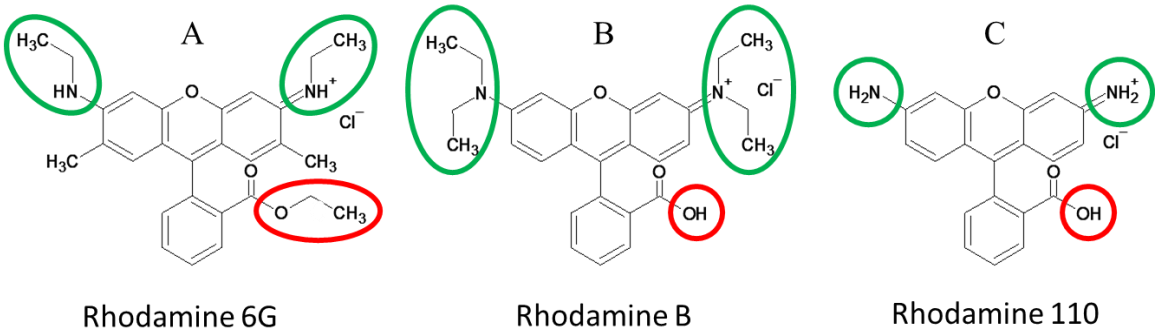

Chart 1.1. The molecular structures of (A) rhodamine 6G, (B) rhodamine B, and (C) rhodamine 110 with emphasis on the functional group differences between the molecules. Circled in green are the amine groups of the rhodamines. R6G has secondary amines, RB has tertiary amines, and R110 has primary amines. Circled in red are the carbonyl functional groups of the rhodamines. R6G has an ethyl ester, whereas RB and R110 have carboxyl groups.

CHAPTER 2

Instrumentation, Methodology, and Characterization

To accomplish the goals outlined in Section 1.5, gold nanoparticles were used as the SERS substrate. The synthesis, aggregation, stabilization, and characterization of the gold nanoparticles used in this study are discussed below, along with the reaction monitoring setup and the computational and data analysis methods that were used.

2.1 Nanoparticle Synthesis

The gold nanoparticle colloid was synthesized using a standard citrate reduction method, similar to the Turkevich method.[33] 120 mg of aurochloric acid ($HAuCl_4 \cdot 3H_2O$, purchased from Sigma-Aldrich) was placed in a 500-mL round-bottom flask. 250 mL of deionized water was then added to the flask, which was swirled by hand until the aurochloric acid was completely dissolved. The resulting yellow solution was placed on a sand bath connected to a variac. A condenser was attached to the flask, then the solution was allowed to heat up. Once the solution began to boil (after approximately 1 hour), 25 mL of aqueous 1% sodium citrate solution was added to the aurochloric acid solution. Immediately, the resulting solution changed color from yellow to colorless to wine red. The solution was refluxed for 1 hour, then allowed to cool to room temperature.

The aurochloric acid served as a source of Au^{3+} ions, which were reduced to Au^0 by reacting with the citrate ions. The resulting neutral gold atoms nucleated and formed spherical gold nanoparticles. The excess citrate ions in solution adsorbed onto the gold nanoparticles' surfaces and served as a weak stabilizing agent, preventing the gold nanoparticles from aggregating together initially. However, SERS performance of the gold nanoparticles begins to decline noticeably after about 3 months.

Additionally, silver-coated gold nanoparticles were synthesized and compared to gold nanoparticles. Literature suggested that silver-coated gold nanoparticles produced a Raman enhancement stronger than pure gold nanoparticles by more than an order of magnitude.[34] Silver-coated gold nanoparticles were synthesized by adding 3 mL of 0.1 M ascorbic acid and 25 mL of 10^{-3} M silver nitrate to 20 mL of gold nanoparticle colloid (synthesis mentioned above). For experiments involving silver-coated gold nanoparticles, identical amounts of analyte and stabilizing agent (if applicable) were added to both types of nanoparticles.

2.2 Nanoparticle Aggregation

As mentioned in Section 1.3, analytes must be located in hot spots to experience Raman enhancement.[35] Hot spots are regions located between two or more adjacent aggregated nanoparticles. At these hot spots, the localized electric field is much higher than the surrounding area, resulting in an inhomogeneous electric field in solution.[16] Due to this inhomogeneous electric field, which is most intense at hot spots, the observed Raman signal of molecules in said hot spots is significantly increased. For analytes to be located in the hot spots, the analytes must adsorb onto the nanoparticles' surfaces, and then the nanoparticles need to be aggregated, typically by addition of a salt.[36] Aggregation of the nanoparticles was induced by the addition of an organic salt analyte (i.e. rhodamine 6G chloride) which simultaneously adsorb to the surfaces of the nanoparticles as they aggregated. Specifically, 200 μL of 4×10^{-3} M aqueous analyte (e.g. rhodamine 6G or rhodamine B) was added to a 10-mL aliquot of as-prepared gold nanoparticle colloid with stirring. The volumes and concentrations of analytes and nanoparticles were optimized to produce maximum Raman intensity while still being resource-efficient.

2.3 Nanoparticle Stabilization

Although aggregation is needed to obtain the enhancement of the analyte's Raman signal, excess aggregation leads to precipitation of the nanoparticle aggregates and causes an overall decline of Raman intensity.[35,36] To prevent over-aggregation, the nanoparticle aggregates must be immobilized onto a surface, or aggregation must be arrested using a stabilizing agent.[23] Stabilizing agents are typically surfactants which adsorb onto the nanoparticles on one end and provide steric hinderance with the other end.[23] Adding a stabilizing agent to the nanoparticles before initiating aggregation will prevent aggregation completely. Adding a stabilizing agent to the nanoparticles after they have over-aggregated will not reverse precipitation in that case. Therefore, the stabilizing agent must be added during the aggregation process to produce semi-aggregated nanoparticles that do not precipitate and, yet, are capable of surface-enhancement via hot spots.

In this study, the aggregation process was arrested using sodium dodecyl sulfate (SDS) to ensure long-term nanoparticle stability. Specifically, 800 μL of a 0.04-M SDS aqueous solution was added immediately after aggregation was initialized, as stated above. The volume and concentration of the stabilizing agent was optimized to achieve maximum Raman signal stability (reduce overall signal decay over time), while still being resource-efficient. Previously, 1-decanethiol was used as the nanoparticle stabilization agent.[37] However, 1-decanethiol had poor water solubility compared to SDS, and it would often separate and float on the water's surface over time. Because SDS was more water soluble and showed better nanoparticle stability results, it was favored over 1-decanethiol.

2.4 Nanoparticle Characterization

To characterize the synthesized gold nanoparticles, UV-visible absorption spectroscopy and transmission electron spectroscopy (TEM) were used. Using UV-visible absorption spectroscopy, the extent of aggregation of the nanoparticles was studied in various conditions. Using TEM, the size and shape of the nanoparticles was observed.

2.4.1 UV-Visible Absorption Spectroscopy

One of the methods used to characterize the nanoparticles before and after aggregation and stabilization was UV-visible absorption spectroscopy. UV-visible spectroscopy is a notable technique since electronic energy transitions often occur in the UV-visible range of the electromagnetic spectrum. Since a plasmon is an electronic transition for a nanoparticle, aggregated or unaggregated, it will be observed in the UV-visible range of the electromagnetic spectrum and can be related to the size and distribution of the nanoparticles present in a colloid (Section 1.4). The UV-visible spectra were measured using a Shimadzu UV-2600 spectrophotometer over the 400-800 nm range with a resolution of 1 nm. Every sample that was analyzed was diluted to a 1/5 concentration to ensure the maximum absorbance value was low enough (below about 1.5) to not be affected by nonlinear absorption effects. UV-visible absorption spectra of aggregated and unaggregated, stabilized and unstabilized nanoparticles are shown in Figure 2.1. The spectra demonstrate the unaggregated nanoparticle peak near 525 nm, which is related to the size of the nanoparticles. As expected, no 700 nm peak (due to the plasmon of nanoparticle aggregates) is seen in the colloid prior to aggregation. Aggregation, with or without stabilization, produces plasmons that absorb at roughly the same wavelength (i.e.

700 nm). When the nanoparticles are not stabilized, the 700 nm peak decreases in absorbance and undergoes a slight red shift over time (discussed more in Section 3.1).

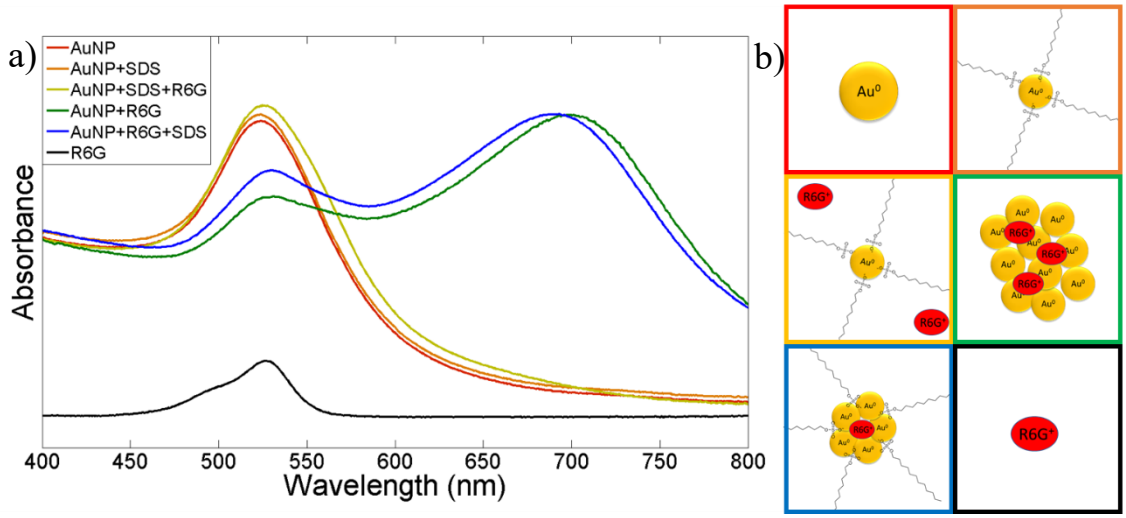

Figure 2.1. UV-visible spectra of the gold nanoparticle colloid: alone (red), with SDS added (orange), with SDS added then R6G (yellow), with R6G added (green), with R6G added then SDS (blue), and just R6G alone (black). Graphical representations of each condition are shown in color-coordinated boxes to the right.

2.4.2 Transmission Electron Microscopy

Nanoparticles were imaged using transmission electron microscopy (JEOL JEM-1400Plus) to obtain their size and shape. To prepare the samples, copper grids were first coated with formvar, then a droplet of nanoparticle solution was placed on a formvar-coated grid. After 5 minutes, the droplet was wicked away using a strip of filter paper, and the sample-loaded grid was inserted into the transmission electron microscope (TEM) for analysis. The TEM images for unaggregated, over-aggregated, and semi-aggregated gold nanoparticles are shown in Figure 2.2. The unaggregated nanoparticles have an average diameter of approximately 30 nm. The over-aggregated nanoparticles formed large masses of nanoparticles, most of which precipitated out of solution. The semi-aggregated nanoparticles formed aggregated clusters consisting of 10-100 nanoparticles, which were much smaller than the over-aggregated nanoparticles. Semi-aggregation allows the

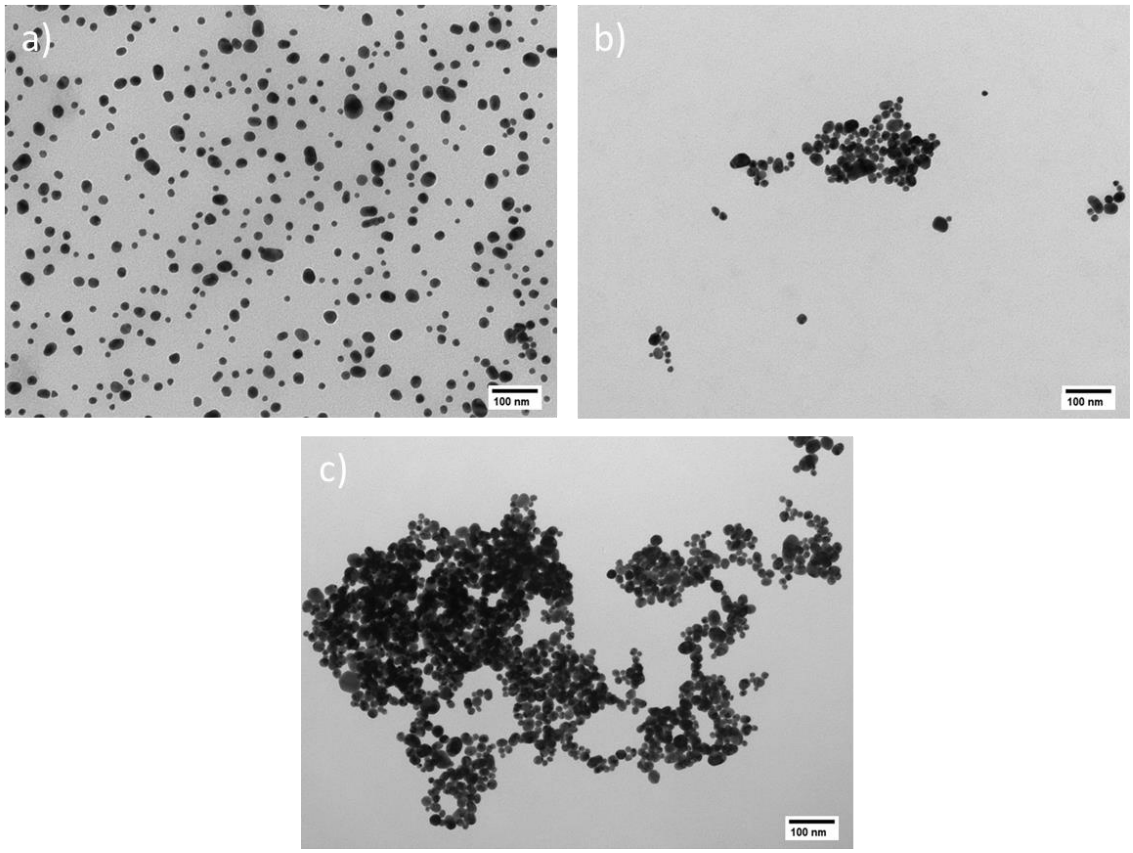

Figure 2.2. TEM images of a) unaggregated, b) semi-aggregated, and c) over-aggregated gold nanoparticles. The unaggregated nanoparticles are mostly individual nanoparticles, whereas over-aggregated and semi-aggregated nanoparticles formed clusters of nanoparticles. The over-aggregated nanoparticle clusters consisted of several thousand nanoparticles, while the semi-aggregated nanoparticles consisted of 10-100 nanoparticles.

nanoparticles to form SERS "hotspots" between neighboring nanoparticles in the clusters without becoming too large and precipitating out of solution.

2.4.3 pH Stability

To test the pH-sensitivity of the stabilized nanoparticles, the nanoparticles were aggregated and stabilized as mentioned above. Then, solutions were adjusted to various levels of pH by the addition of a few hundred microliters of 0.1 M HCl or NaOH. The pH-sensitivity was explored at pH levels of 3, 4.5, 5.6 (control), 9, and 11 by collecting a

UV-visible spectrum every 30 minutes for 6 hours. The pH of each solution was checked by using an Oakton pH Testr 10.

2.5 Reaction Monitoring Setup

To monitor reactions, a peristaltic flow system was used (Figure 2.3). The nanoparticle colloid, analyte, and stabilizing agent were added to the reaction vessel (RX) which was stirring on a stir plate. The solution from that reaction vessel was transferred through tubes using a peristaltic pump (PUMP) to the flow cuvette (C) where a Raman probe collects Raman spectra. Raman spectra were measured from 400-1700 cm^{-1} with 1 cm^{-1} resolution on a backscatter-collecting, probe-type spectrometer (Agiltron Peakseeker-L) with an excitation wavelength of 785 nm at 300 mW, with 10-s integration times.

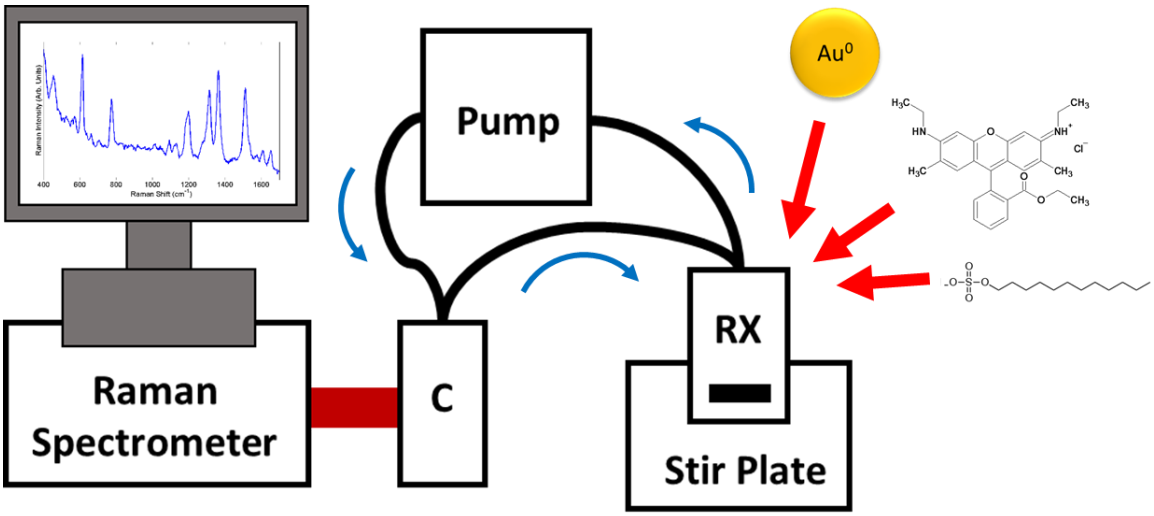

Figure 2.3. The reaction monitoring set up, consisting of a reaction vessel (RX) on a stir plate, a peristaltic pump (Pump), and a flow cuvette (C). The direction of flow is indicated by the blue arrows.

2.6 Data Processing and Analysis

Custom MatLab codes were used to extract, process, and plot experimental and computational data. For experimental Raman spectra, Matlab was used to plot several

spectra on the same set of axes and to plot peak area versus time. The peak areas were calculated for selected peaks by fitting a Gaussian curve to each peak then integrating. All Raman spectra were normalized to correct for a changing baseline.

Similarly, for UV-visible spectra, Matlab was used to plot several spectra on the same set of axes and to plot normalized peak areas versus time. The peak areas were calculated by using trapezoidal integration between selected bounds. When the peak areas were plotted over time, they were all divided by the initial peak area so that the first peak area was normalized to a value of 1 and every following value was relative to that point. Matlab was used to plot the calculated vibrational frequencies as a theoretical Raman spectrum (Raman intensity versus Raman shift) and to compare the resulting spectra to experimental data.

CHAPTER 3

Results and Discussion

The gold nanoparticles used for SERS were stabilized and optimized, then used to monitor and study a reaction between R6G and OH^-. Reaction monitoring consisted of attempting to determine the kinetics and reaction mechanism of the reaction. Silver-coated gold nanoparticles were also briefly studied and compared to pure gold nanoparticles as a potential SERS substrate replacement.

3.1 Nanoparticle Stabilization

Peak areas of several peaks in the Raman spectrum of R6G on stabilized and unstabilized nanoparticles as a function of time are shown in Figure 3.1. Using unstabilized nanoparticles, the overall Raman intensity and peak areas decreased sharply over time, which is attributed to nanoparticle over-aggregation and subsequent precipitation (Figure 3.1a and b). The four most intense Raman peaks (614 cm^{-1}, 1313 cm^{-1}, 1364 cm^{-1}, and 1513 cm^{-1}) were monitored over 30 minutes by plotting their peak areas versus time. The peak areas were calculated using a custom Matlab code that fitted each peak with a Gaussian curve and integrated (discussed in Section 2.6). Using stabilized nanoparticles, the overall Raman intensity and peak areas remained relatively constant (Figure 3.1c and d). The same four Raman peaks were monitored over the same amount of time using stabilized nanoparticles and exhibited a peak area decrease of less than 10%. Similar results were obtained for rhodamine B and rhodamine 110.

While monitoring the 700 nm peak in UV-visible spectra over time for stabilized and unstabilized nanoparticles, the same trend was observed (Figure 3.1e). The blue trace and green trace in Figure 3.1e correspond to the conditions described in Figure 2.1 (blue

and green traces, respectively). Although initially both conditions look nearly identical (both have peaks at 525 nm and 700 nm with similar absorbance), over time the peak area of the 700 nm peak of the unstabilized nanoparticles (i.e. the green trace) decreased,

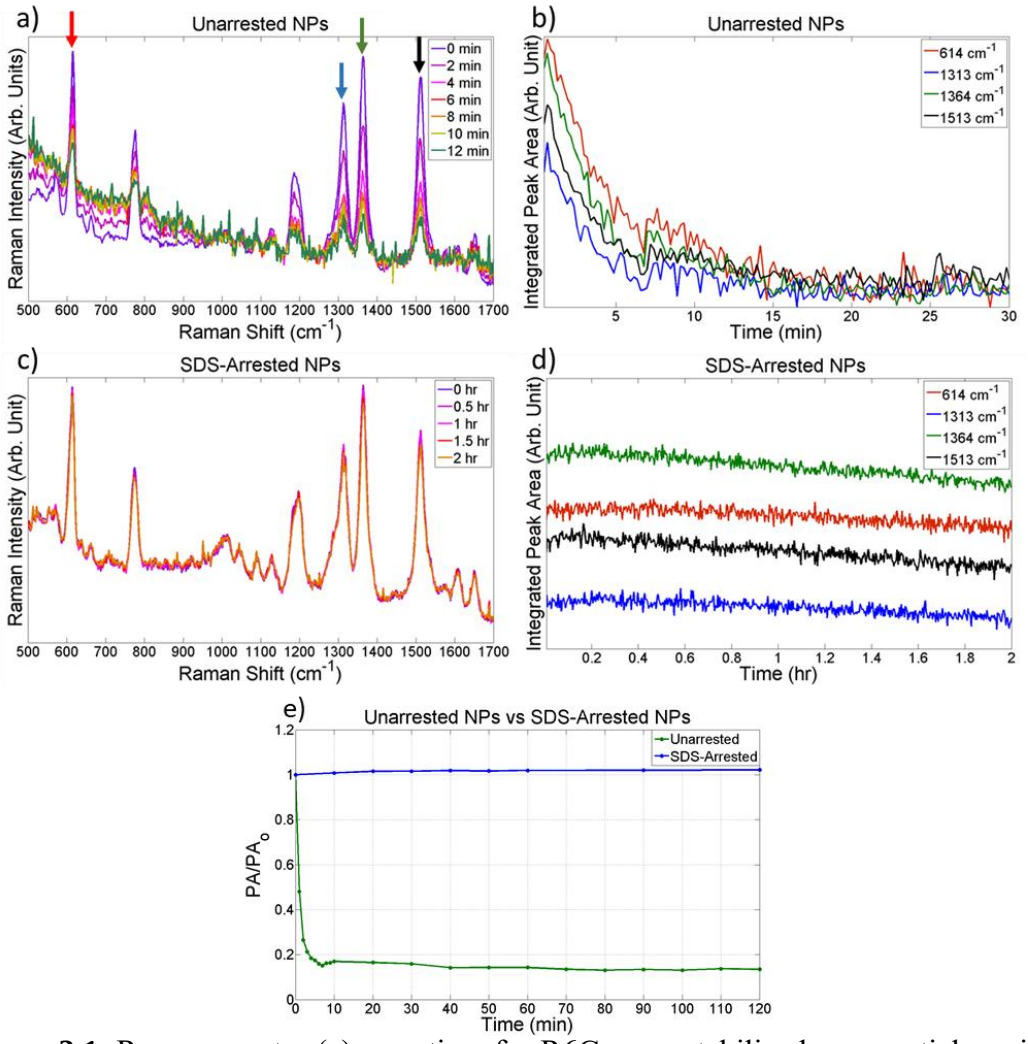

Figure 3.1. Raman spectra (a) over time for R6G on unstabilized nanoparticles with no reaction occurring. The Raman spectra shown are from every 2 minutes. Color-coordinated arrows are pointing to the peaks whose peak areas were tracked (b) for 30 minutes. (Red is 614 cm^{-1}, blue is 1313 cm^{-1}, green is 1364 cm^{-1}, and black is 1513 cm^{-1}). Raman spectra (c) over time for R6G on SDS-stabilized nanoparticles with no reaction occurring. The Raman spectra shown are from every 30 minutes. d) The peak areas of the same Raman peaks from b) as a function of time for 2 hours. e) The normalized peak area in the UV-visible spectra of the 700 nm peak as a function of time for stabilized (blue) and unstabilized (green) nanoparticle aggregates (2 hours).

whereas the peak area of the 700 nm peak of the stabilized nanoparticles (i.e. the blue trace) remained stable. The sharp decrease of absorbance in the UV-visible spectrum of the unstabilized nanoparticles is attributed to over-aggregation of the nanoparticles. As the nanoparticles precipitated, the solution became olive green and more transparent.

3.2 Nanoparticle pH-Stability

As a demonstration of the pH-resistance of these stabilized nanoparticles, the peak areas of the 700 nm peak in the UV-visible spectra of stabilized nanoparticles with various pH values (ranging from 3 to 11) were monitored over 6 hours (Figure 3.2). The peak areas did not change appreciably as a function of time for any of the tested pH values. Because changes in peak area are attributed to nanoparticle precipitation and there is very little change to the peak areas of stabilized nanoparticles, any changes to the Raman spectra during a reaction (using stabilized nanoparticles) are attributed to changes in the molecular structure of the analyte, not to degradation, aggregation, or other alteration of the gold nanoparticles.

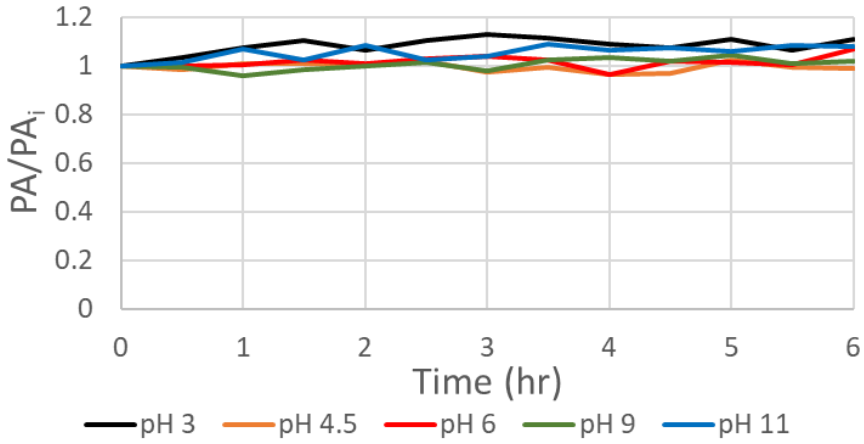

Figure 3.2. The normalized peak area (700 nm) as a function of time for pH 3 (black), pH 4.5 (orange), pH 5.6 (control; red), pH 9 (green), and pH 11 (blue) for 6 hours.

3.3 Raman Intensity Concentration Dependence with a Carbon Disulfide Internal Standard

Carbon disulfide (CS_2) was briefly used as an internal standard in Raman spectra to more accurately compare Raman spectra from different conditions. Figure 3.3a shows the Raman spectra of different concentrations of R6G with the same amount of CS_2. The three most intense Raman peaks for R6G (i.e. 615 cm^{-1}, 1312 cm^{-1}, and 1364 cm^{-1}) were used in conjunction with the CS_2 peak at 632 cm^{-1} to analyze the effect of concentration on Raman intensity by taking the ratio of the peak area of the R6G peaks to the peak area of the CS_2 peak. This ratio was plotted against the log of the concentration of R6G (Figure 3.3b). Because the same amount of CS_2 was used in each trial, the concentration of CS_2 in the colloid was the same, which means, ideally, the intensity of the CS_2 peak should have been the same in each trial. Taking the ratio of R6G peaks and the CS_2 peak was done to account for the different intensity of the CS_2 peak in each trial. All three R6G/CS_2 ratios followed the same trend; peak areas decreased as R6G concentration decreased. Although the most concentrated trial had the highest peak area ratios, the second most concentrated trial was determined to be the best concentration to

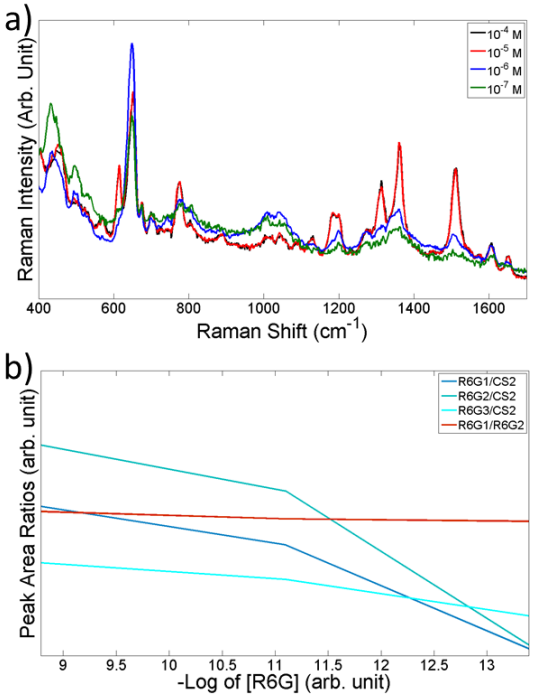

Figure 3.3. a) Raman spectra of R6G at different concentration with the same concentration of CS_2 as an internal standard. b) Peak area ratios over time. R6G1 is 615 cm^{-1}, R6G2 is 1312 cm^{-1}, and R6G3 is 1364 cm^{-1}.

use for other experiments since both concentrations offered similar signal to noise. Although using CS_2 as an internal standard provided a way of comparing the Raman spectra from different experiments, the peak intensity of the CS_2 Raman peak decreased rapidly over a span of 30 min (much faster than the over Raman intensity decrease) and the ratio of peak areas was not quantitative (i.e. R6G concentration and the peak ratios did not increase or decrease linearly). For this reason, CS_2 was not used for timed experiments since it was not an adequate internal standard over long periods of time.

3.4 Nanoparticle Aggregation Optimization

It became apparent that the nanoparticles aggregated at a slower rate when using RB and R110 compared to using R6G. This slower aggregation was affected when SDS was added to arrest the aggregation process; therefore, the time between initiating aggregation and stabilization was optimized for each analyte. By monitoring the UV-visible spectra and Raman spectra during the nanoparticle aggregation process for each analyte, the optimum moment to add SDS was determined by observing when the plasmon peak (700 nm) in the UV-visible spectrum reached a maximum and when the Raman intensity reached a maximum in the Raman spectrum. Figure 3.4a, 3.4c, and 3.4e exhibit the gold nanoparticle's UV-visible spectra over time with R6G, RB, and R110 added, respectively. The plasmon peak (700 nm) reached a different maximum absorbance for each analyte. Figure 3.4b, 3.4d, and 3.4f display the peak areas of various peaks for R6G, RB, and R110, respectively. The peak areas of each analyte reached maximums at similar times as their UV-visible spectra. The optimum point to add SDS to the nanoparticle colloid for R6G was 1 sec after adding R6G. For RB and R110, the optimum time was 2 minutes

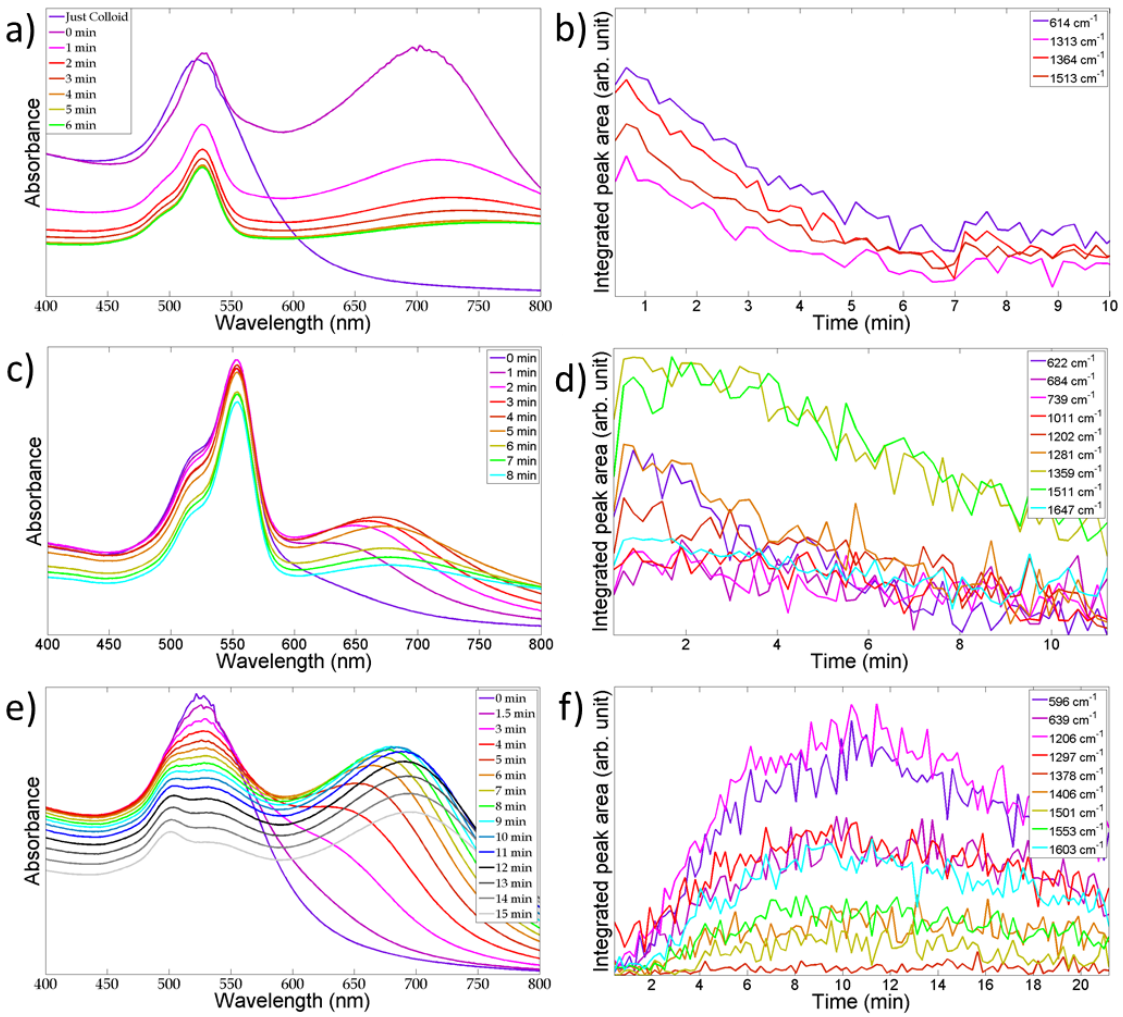

Figure 3.4. a), c), and e) show the UV-visible spectra over time of the gold nanoparticles with R6G, RB, and R110 added, respectively. b), d), and f) show the peak areas of various peaks for R6G, RB, and R110, respectively.

and 8 minutes, respectively. Although the reason why R6G, RB, and R110 aggregate the nanoparticles at different rates is not fully understood, it seems reasonable to suspect that the differences are due to their molecular structure. Generally, the accepted cause of nanoparticle aggregation is increasing ionic strength,[36] but since R6G, RB, and R110 have the same charge and concentration, ionic strength must not be the cause for the observed different aggregation rates in this case. Since R6G has secondary amines, RB has tertiary amines, and R110 has primary amines, one would expect RB and R110 to be the extremes

of aggregation rate (i.e. R110 < R6G < RB or R110 > R6G > RB). Because that is not the case, the difference in nanoparticle aggregation rates are independent of the amine groups of the rhodamines, leaving only the carboxyl groups as the likely reason.

Because R110 aggregated the nanoparticles much slower than the other analytes, TEM was used to visualize the aggregation process (Figure 3.5). Since the plasmon peak and Raman intensity reach a maximum around 8 min, four nanoparticle samples were made: before the addition of R110 (Figure 3.5a), 3 min after the addition of R110 (Figure 3.5b), 8 min after the addition of R110 (Figure 3.5c), and 12 min after the addition of R110 (Figure 3.5d). SDS was added to each sample at the described times and stirring was

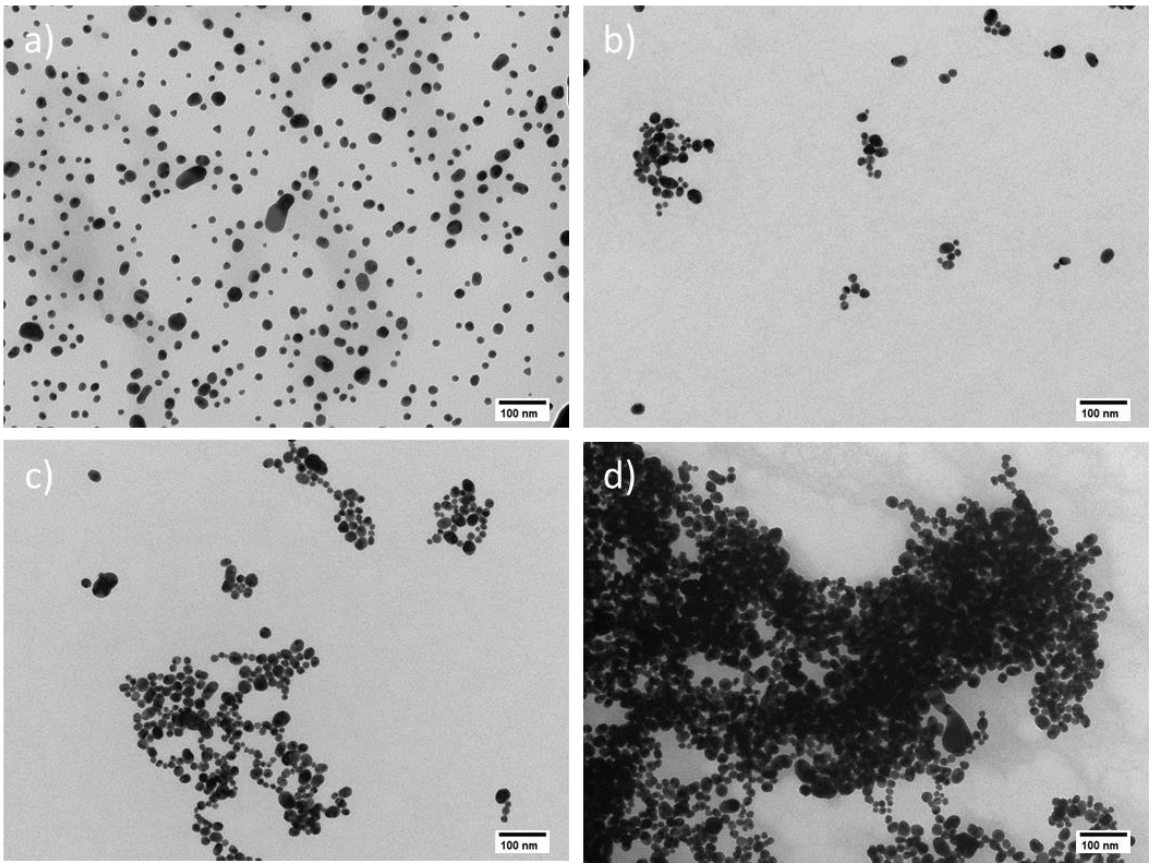

Figure 3.5. TEM images of the nanoparticle colloid a) without the addition of R110, b) 3 min after the addition of R110, c) 8 min after the addition of R110, and d) 12 min after the addition of R110.

stopped to prevent further aggregation. As expected, there was no nanoparticle aggregation when R110 was not added to the colloid. Additionally, comparing Figure 3.5b, 3.5c, and 3.5d, the nanoparticle aggregate size increased as aggregation time increased. 3 min after the addition of R110 resulted in the smallest aggregates, while the largest aggregates occurred after 12 min. Relating the TEM images to the Raman peak area over time, as the nanoparticles aggregate the Raman signal from R110 increases as more hot spots are created. Eventually a maximum intensity is achieved right before the nanoparticle aggregates become too large and start to precipitate from solution, resulting in the Raman intensity to decline over time. For R6G, RB, and R110 this optimum time is 1 sec, 2 min, and 8 min, respectively, in excellent agreement with the plasmon timing experiments.

3.5 Observed Reaction Between R6G and OH^-

While evaluating the pH-stability of the nanoparticles (Section 3.2), several changes in the Raman spectrum of R6G were observed at pH 9 and above. Specifically, peaks at 600 cm^{-1}, 1405 cm^{-1}, 1444 cm^{-1}, 1480 cm^{-1} appeared and increased over time while peaks at 615 cm^{-1}, 1313 cm^{-1}, 1364 cm^{-1}, and 1513 cm^{-1} decreased over time (Figure 3.6). Additionally, the presence of an isosbestic point at 610 cm^{-1} (Figure 3.6a) further suggests a reaction occurred. After this observation, several experiments were conducted to

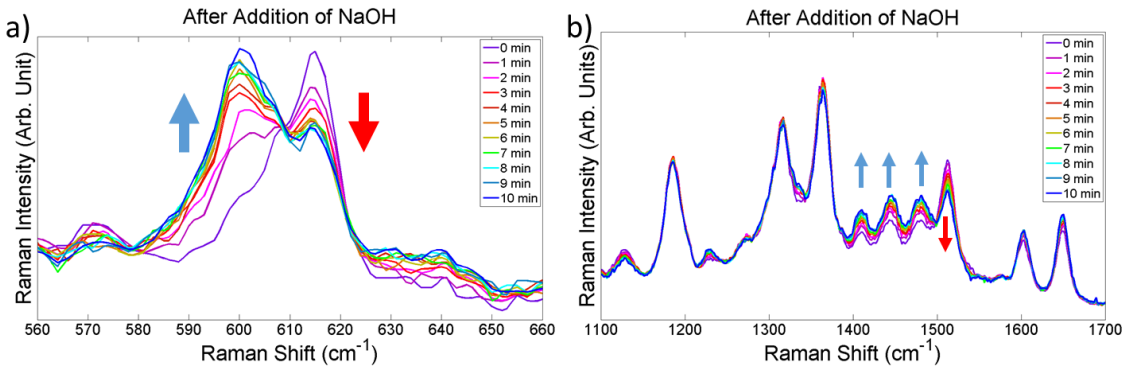

Figure 3.6. Raman spectra over time at pH 11.7 from a) 560 cm^{-1} to 660 cm^{-1} and b) 1100 cm^{-1} to 1700 cm^{-1}.

determine what the reaction was by trying to reproduce the same spectral changes using different conditions.

3.6 Possible Mechanism #1: Saponification (Ester Hydrolysis)

Based on the molecular structure of R6G, the first hypothesized reaction with OH^- was saponification (due to the ethyl ester on R6G). In saponification an ester is converted into a carboxylic acid under basic conditions (Scheme 3.1). If the reaction in question is saponification, then in acidic conditions esterification should occur (the reverse reaction of saponification). To test this, the Raman spectrum of R6G was observed after adjusting the pH to basic conditions by adding NaOH and then again after adjusting the pH to acidic conditions by adding HCl (Figure 3.7a and b). Adjusting the pH to acidic conditions resulted in the Raman peaks at 600 cm^{-1}, 1405 cm^{-1}, 1444 cm^{-1}, 1480 cm^{-1} (i.e. the peaks that appeared after adding NaOH) disappearing, but the original Raman peaks (615 cm^{-1}, 1313 cm^{-1}, 1364 cm^{-1}, and 1513 cm^{-1}) did not increase back to their initial intensity. The disappearance of the new peaks suggests that the product formed during the reaction was consumed when the solution became acidic, but the fact that the original peaks did not return to their initial intensity suggests that the reactant (R6G) was not reformed when the product was consumed. These findings did not support the saponification hypothesis, suggesting a second reaction may take place after the solution became acidic.

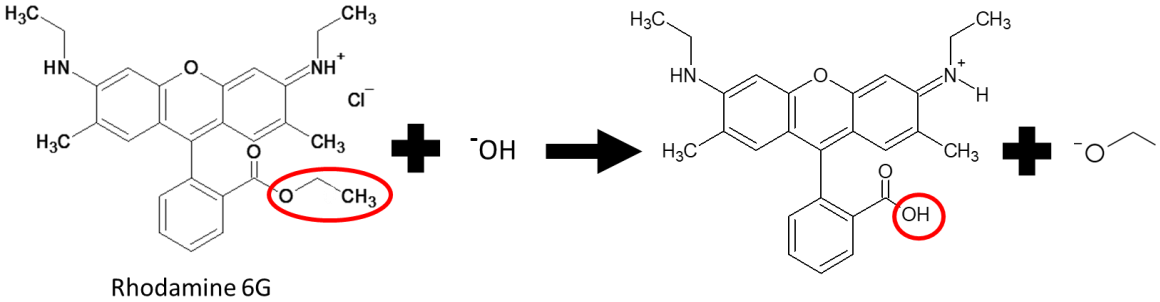

Scheme 3.1. Saponification of R6G. The ethyl ester on R6G is converted into a carboxylic acid.

Additionally, the Raman spectra of RB and R110 were observed under analogous conditions as R6G (Figure 3.7c, d, e, and f). Since RB and R110 do not possess an ester functional group, they cannot undergo saponification; therefore, no changes should be observed in their Raman spectra. However, the Raman spectra of RB and R110 changed similarly to R6G under the same conditions. Both RB and R110 had spectral feature

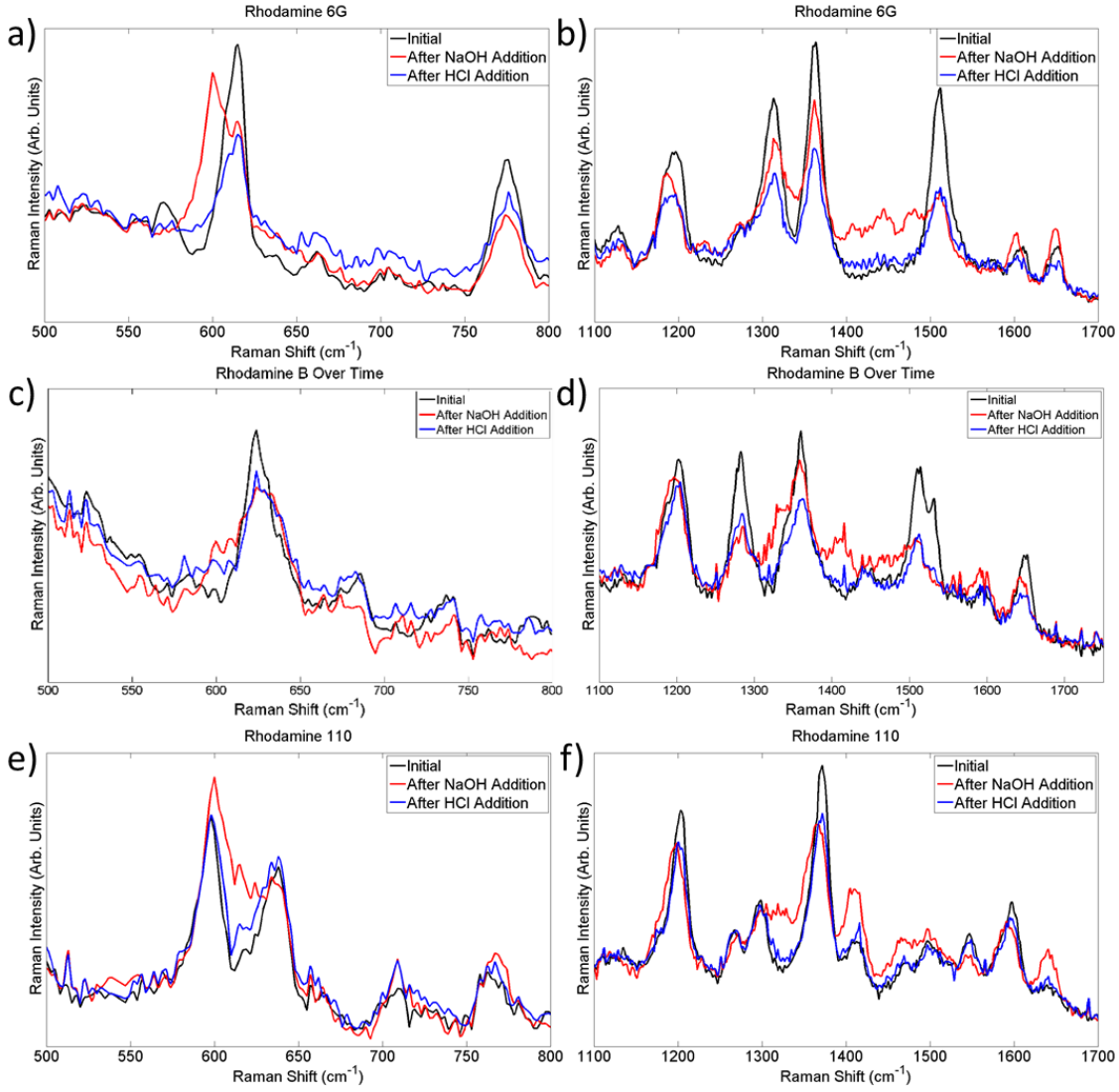

Figure 3.7. Raman spectra of a) R6G from 500-800 cm^{-1}, b) R6G from 1100-1700 cm^{-1}, c) RB from 500-800 cm^{-1}, d) RB from 1100-1700 cm^{-1}, e) R110 from 500-800 cm^{-1}, and f) R110 from 1100-1700 cm^{-1}. For each analyte, the pH of the solution was changed to basic and then acidic.

increase around 600 cm^{-1} and between 1400-1500 cm^{-1} while original peaks seemed to decrease. The observation of changes to the Raman spectra of RB and R110 does not support the saponification hypothesis and suggests RB and R110 may undergo a similar reaction as R6G.

Two more experiments were conducted to investigate the saponification hypothesis: adding a relatively large amount of 1) methanol and 2) phenol the reaction mixture. The goal of these experiments was to replace the ethyl ester on R6G with an ester of a different type (i.e. a methyl group and phenyl group, respectively) by using an excess amount of alcohol. By replacing the alkyl group of the ester on R6G, changes around 600 cm^{-1} and 1400-1500 cm^{-1} in the Raman spectrum of R6G were expected. If changes were observed in these regions by replacing the alkyl group of the ester, then those regions are likely related to vibrational modes involving the carbonyl group of R6G, which would support the saponification hypothesis. Initially, methanol was used, forming R6G-methyl ester if successful. R6G was once again subject to basic conditions then acidic conditions but with methanol present at 100-fold the concentration of R6G. With methanol present in such a high concentration, the formation of R6G-methyl ester should have been highly favored based on Le Chatelier's Principle. However, the Raman spectra looked identical to Figure 3.7a and 3.7b, suggesting methanol played no role in the reaction. Due to the similar structure of the R6G-methyl ester and R6G-ethyl ester (therefore likely having similar vibrational modes), this procedure was repeated with the use of phenol present at a concentration 100-fold that of R6G. The vibrational modes of R6G-phenyl ester should differ from R6G-ethyl ester to a greater extent, making it potentially more noticeable in the Raman spectrum. However, the same results were obtained as the methanol experiment,

indicating R6G-phenyl ester was not formed and saponification/esterification was not occurring.

According to the literature, the hydrolysis of the ethyl ester on R6G forms rhodamine 19 (R19) which was conducted in a NaOH/EtOH mixture with heating for 1 hour.[38] Given that the saponification of R6G in the literature requires heating for 1 hour, whereas in this study no heat was applied, it is very unlikely for saponification to be the reaction that was observed between R6G and OH^-.

3.7 Possible Mechanism #2: Dimerization

R6G dimerization was the second possible explanation for the changes in the Raman spectrum in basic pH. Dimerization is the process of two monomers forming a stable complex together (Scheme 3.2). For R6G, dimerization in water is promoted when concentration[39–41] or ionic strength[42] is increased. R6G should not dimerize due to increasing pH,[43] so initially it was assumed that adding NaOH increased ionic strength which caused the changes in the Raman spectrum (dimerization). Work by several groups[39–43] suggests that the absorbance peak at 520 nm is due to the monomer form of

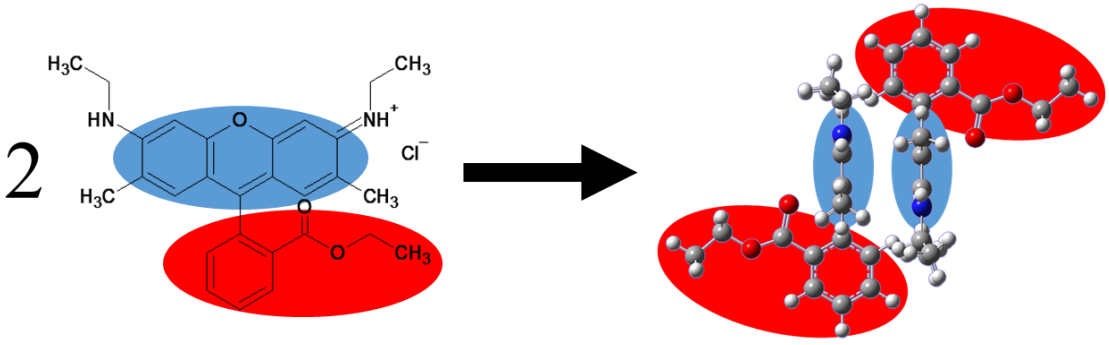

Scheme 3.2. Dimerization of R6G. Two R6G molecules form a stable complex (dimer). The xanthene ring of R6G has been highlighted in blue, and the phenyl group has been highlighted in red. After dimerization, the xanthene rings of the two R6G molecules are face-to-face, and the phenyl groups are perpendicular to xanthene rings, facing away.

R6G while the shoulder peak at 500 nm is due to the dimer form of R6G. Figure 3.8a displays the UV-visible spectra of aqueous R6G (no gold nanoparticles) at concentrations ranging from 0.5×10^{-5} M to 2.5×10^{-5} M. As concentration increased, the 500 nm peak increased representing the formation of R6G dimers in solution. Figure 3.8b displays the Raman spectra of R6G at 1×10^{-4} M (with gold nanoparticles) over time. The goal for this experiment was to produce the peaks at 600 cm^{-1}, 1405 cm^{-1}, 1444 cm^{-1}, and 1480 cm^{-1} by increasing the concentration well beyond the amount needed to form dimers. If the new peaks were a product of dimerization, then they should have appeared. The Raman spectrum was tracked over 2 hours in case the process was slow. Because increasing the

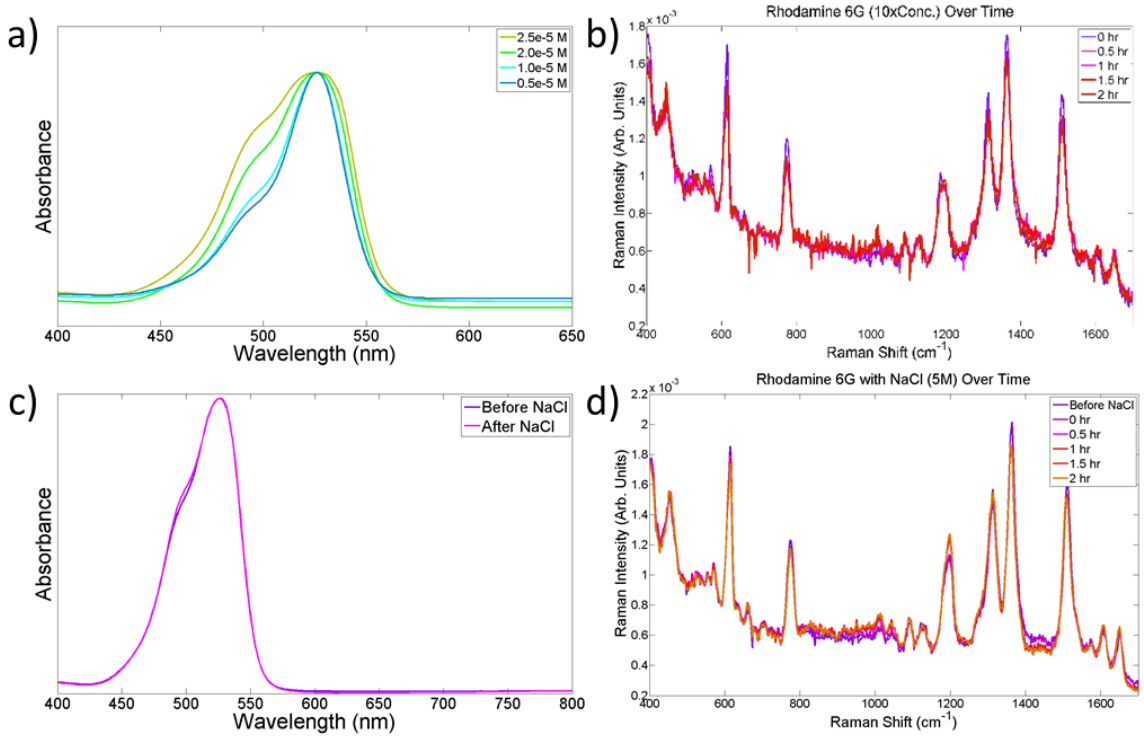

Figure 3.8. a) UV-visible spectra of R6G at 0.5×10^{-5} M, 1.0×10^{-5} M, 2.0×10^{-5} M, and 2.5×10^{-5} M without using nanoparticles. b) The Raman spectra over time for R6G at 1×10^{-4} M with nanoparticles (a 10-fold increase in concentration relative to the usual amount). c) UV-visible spectra of R6G at 1.0×10^{-5} M before and after adding NaCl (without using nanoparticles). d) The Raman spectra over time for R6G at 1×10^{-5} M (with nanoparticles) with 5 M NaCl added.

R6G concentration passed 2.0×10^{-5} M was shown to form dimers based on the increase in the absorbance peak at 500 nm (Figure 3.8a), having a R6G concentration of 1×10^{-4} M should have formed dimers. If the Raman peaks at 600 cm^{-1}, 1405 cm^{-1}, 1444 cm^{-1}, and 1480 cm^{-1} were caused by dimerization, then those peaks would have appeared in Figure 3.8b. Those Raman peaks did not appear, suggesting the dimerization mechanism is not the correct mechanism.

Since ionic strength is known to promote dimerization of R6G,[42] 5-M NaCl was used to increase the ionic strength of the R6G solution, then it was monitored using UV-visible spectroscopy (no gold nanoparticles, Figure 3.8c) and using Raman spectroscopy (with gold nanoparticles, Figure 3.8d). In the UV-visible spectrum, the dimer peak (500 nm) was not reproduced by high ionic strength. In the Raman spectrum, the new peaks (600 cm^{-1}, 1405 cm^{-1}, 1444 cm^{-1}, 1480 cm^{-1}) were not reproduced either from high ionic strength.

Dimerization of R6G is influenced by increasing concentration or increasing ionic strength. However, neither of those experiments resulted in the appearance of the Raman peaks at 600 cm^{-1}, 1405 cm^{-1}, 1444 cm^{-1}, and 1480 cm^{-1}, suggesting dimerization is not the correct mechanism for the reaction between R6G and OH^-.

3.8 Possible Mechanism #3: Amine Deprotonation-Nucleophilic Attack

The third hypothesis for the reaction between R6G and OH^- was deprotonation of the positively charged amine on R6G. This deprotonation would result in the nitrogen of the amine group becoming more nucleophilic, which could allow R6G to undergo a second reaction, such as a nucleophilic attack (Scheme 3.3). If deprotonation of the amine group is occurring, then only R6G and R110 would be able to undergo the reaction, since they

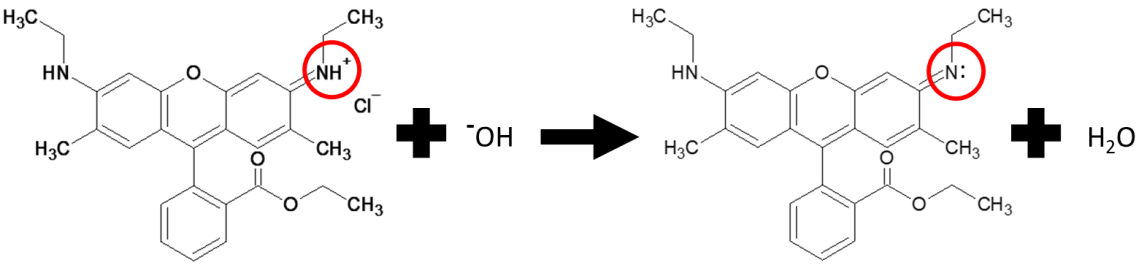

Scheme 3.3. Deprotonation of R6G. R6G is normally a cation due to the positively charged amine group (circled in red). After deprotonation, this amine group would lose the positive charge, resulting in R6G being neutral.

possess secondary and primary amines, respectively. RB has a tertiary amine, which cannot be deprotonated.

To gain more information about the reaction the absorbance peak of R6G, RB, and R110 were monitored over time using UV-visible spectroscopy (Figure 3.9). Since excitations in the visible range of the electromagnetic spectrum are related to electronic transitions of a molecule, changes in the absorbance peak for R6G, RB, and R110 can be related to their conjugated pi-systems, to which their amine groups belong. During the first 90 min of monitoring, each solution was at pH 10, then the pH was adjusted back to pH 6 and monitored for 90 more minutes. The normalized peak area was plotted versus time such that the peak area of the absorbance band before pH adjustment was 1. For R6G (Figure 3.9a) in basic pH, the absorbance peak decreased initially for 30 min, then increased immediately after adjusting to an acidic pH. The initial decay of the absorbance peak in basic pH for R6G could be due to the deprotonation of an amine group. Similarly. the immediate increase of the absorbance peak in acidic pH could be related to the re-protonation of said amine group. The absorbance does not return to its initial value, suggesting another reaction took place such that some of the deprotonated R6G was

consumed. For RB (Figure 3.9b) in basic and acidic pH, the absorbance peak did not change much over both 90-min intervals. Since RB has tertiary amines, it cannot undergo deprotonation at those sites. For R110 (Figure 3.9c) in basic pH, the absorbance peak increases greatly in basic pH and stays constant for the rest of the 90 minutes. In acidic pH the absorbance peak for R110 did not seem to change. Although the expected results for R110 were for its absorbance peak to decrease in basic pH and increase in acidic pH (similar to R6G), seeing any change in the absorbance peak of R110 in basic pH suggests something is occurring that involves the conjugated pi-system of R110, which could be deprotonation of an amine group. In summary, R6G and R110 experienced changes in their UV-visible absorbance spectra when NaOH was added to solution, and RB did not experience any changes. These observations support the deprotonation reaction mechanism because RB cannot be deprotonated at the amine groups, whereas R6G and R110 can.

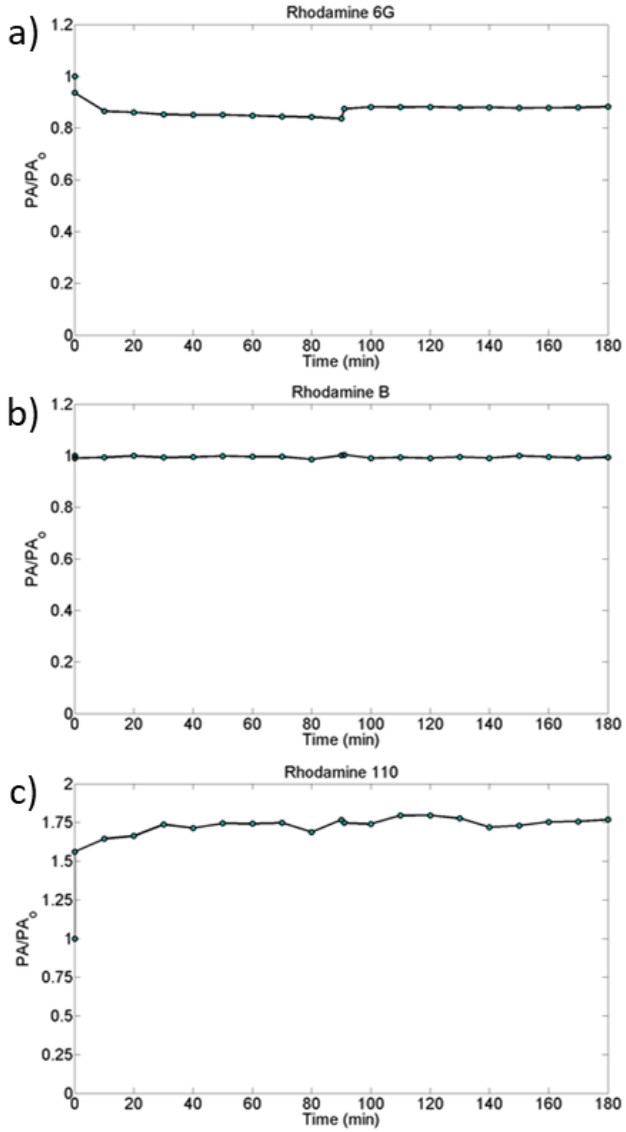

Figure 3.9. Normalized peak area over time for a) R6G, b) RB, and c) R110. NaOH was added at 0 minutes (pH 10), and HCl was added at 90 minutes (pH 6).

3.9 Silver-Coated Gold Nanoparticles versus Pure Gold Nanoparticles

Briefly, silver-coated gold nanoparticles were tested for Raman enhancement and stability with the intent of eventually replacing pure gold nanoparticles. The silver-coated gold nanoparticles were synthesized simply by adding silver nitrate and ascorbic acid to already-prepared pure gold nanoparticles. Using R6G as a model analyte, the SERS signal for R6G on silver-coated gold nanoparticles was compared to the SERS signal for R6G on pure gold nanoparticles (Figure 3.10a). The absolute intensity of silver-coated gold nanoparticles was about 5-fold the intensity of pure gold nanoparticles. Monitoring several of the Raman peaks over time (614 cm^{-1}, 774 cm^{-1}, 1313 cm^{-1}, 1364 cm^{-1}, 1513 cm^{-1}, and 1652 cm^{-1}) for unstabilized silver-coated gold nanoparticles revealed that the peak areas did not decay over 2.5 hr (Figure 3.10b). For the peaks at 774 cm^{-1} and 1364 cm^{-1}, the peak area gradually increased over time.

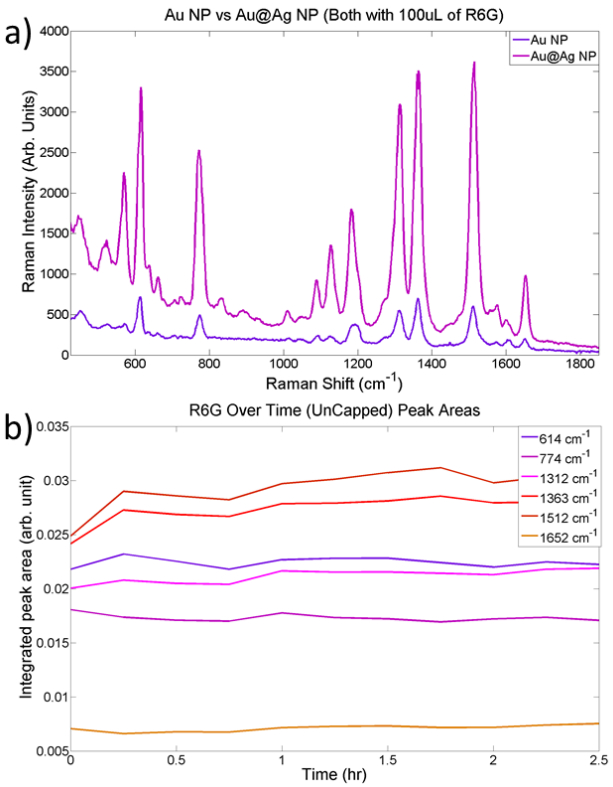

Figure 3.10. a) Raman spectra of R6G on pure gold nanoparticles (purple) and silver-coated gold nanoparticles (magenta). b) Peak areas over time of R6G on silver-coated gold nanoparticles (no SDS).

3.10 Summary

Overall, SDS-stabilized gold nanoparticles were shown to be stable in solution for at least 2 hours. It is important to add SDS at the right time after adding an aggregating agent or

analyte, because different analytes aggregate the nanoparticles at different rates. Using only SERS and UV-visible spectroscopy, the reaction between R6G and OH^- seems to most likely be amine deprotonation followed by a second reaction.

CHAPTER 4

Conclusions and Future Work

Surface-enhanced Raman spectroscopy (SERS) offers great advantages for reaction monitoring compared to other methods. Namely, SERS offers great sensitivity, selectivity, time resolution, and low water interference. For these reasons, interest in SERS as a reaction monitoring technique has been rising. However, monitoring reactions *in situ* using SERS has been challenging due to reduction in nanoparticle stability over time. Surfactants have been used to remedy this difficulty. The objective of this research project was to use surfactant-stabilized gold nanoparticles to successfully monitor a reaction in situ and determine its potential reaction mechanism. Sodium dodecyl sulfate (SDS) was shown to efficiently and easily improve nanoparticle stability. After proving nanoparticle stability, a reaction was chosen to prove the feasibility of SERS as a reaction monitoring technique. The chosen reaction was between rhodamine 6G (R6G) and hydroxide ion due to convenience and its absence in the literature.

Over the course of this research project, it became apparent that the analyte-driven aggregation of the nanoparticles occurred at different rates depending on the analyte. This discovery led to the realization that the nanoparticles had to stabilized at different times depending on the analyte that was being studied. This also brings into question whether unsuccessful attempts to obtain SERS signal on new analytes were actually unsuccessful, or if they just aggregated the nanoparticles slowly. The mechanism for why the nanoparticle aggregation rate is analyte dependent remained unknown.

This study showed that the reaction between R6G and OH^- ion was successfully monitored over time; however, determining reaction kinetics and reaction mechanisms

proved to be more challenging than originally expected. Although the spectral areas of Raman peaks could be plotted over time to track the reaction progress, peaks that were too close in proximity to each other (such as 600 cm^{-1} and 615 cm^{-1} in R6G's Raman spectrum) could not give accurate kinetics with the data analysis method that was used.

The possible reaction mechanism was determined through a process-of-elimination method. The three potential reaction mechanisms were saponification, dimerization, and deprotonation followed by an amine-attack. Using only SERS and UV-visible spectroscopy, saponification and dimerization were eliminated as potential mechanisms through a variety of control experiments. The evidence from the control experiments most supported the deprotonation hypothesis. Determining the reaction that follows deprotonation would require more elaborate control experiments or the use of an established reaction monitoring method. The absence of this reaction in the literature meant that the results from this study could not be compared to published work.

Ways to further this research would be to improve the method of determining kinetics such that the results are more quantitative. Perhaps "residual Raman spectra" could be monitored instead of plain Raman spectra. Residual Raman spectra could be produced by taking the first Raman spectrum in a series of Raman spectra, and subtracting its intensities from the following spectra. By doing this, the differences between the initial spectrum and every subsequent spectrum can be visualized, potentially eliminating most of the noise and allowing more accurate peak fitting and tracking.

Another way to build on the results of this study would be to use an established reaction monitoring method as a benchmark. LC-MS would be recommended due to the type of information that can be obtained from it. Mass spectrometry would help immensely

with identifying the product(s) based on their maximum molar mass and their fragmentation pattern. Mass spectrometry is often used as a characterization method to identify the products of organic reactions, which is precisely the situation presented here. Knowing the exact product(s) that are formed from the reaction between R6G and OH^- would greatly assist in determining the reaction mechanism.

REFERENCES

(1) De Beer, T.; Burggraeve, A.; Fonteyne, M.; Saerens, L.; Remon, J. P.; Vervaet, C. Near Infrared and Raman Spectroscopy for the In-Process Monitoring of Pharmaceutical Production Processes. *Int. J. Pharm.* **2011**, *417* (1–2), 32–47.

(2) Zaikin, V. G. Chromatography-Mass Spectrometry. *J. Anal. Chem.* **2011**, *66* (11), 1090–1094.

(3) Jameson, C. J. Gas-Phase NMR Spectroscopy. *Chem. Rev.* **1991**, *91*, 1375–1395.

(4) Küppers, M.; Heine, C.; Han, S.; Stapf, S.; Blümich, B. In Situ Observation of Diffusion and Reaction Dynamics in Gel Microreactors by Chemically Resolved NMR Microscopy. *Appl. Magn. Reson.* **2002**, *22* (2), 235–246.

(5) Ishima, R.; Torchia, D. A. Protein Dynamics from NMR. *Nat. Struct. Biol.* **2000**, *7* (9), 740–743.

(6) Joung, J. F.; Kim, S.; Park, S. Cationic Effect on the Equilibria and Kinetics of the Excited-State Proton Transfer Reaction of a Photoacid in Aqueous Solutions. *J. Phys. Chem. B* **2018**, *122* (19), 5087–5093.

(7) Santiago, R.; Lemus, J.; Moya, C.; Moreno, D.; Alonso-Morales, N.; Palomar, J. Encapsulated Ionic Liquids to Enable the Practical Application of Amino Acid-Based Ionic Liquids in CO_2 Capture. *ACS Sustain. Chem. Eng.* **2018**, *6* (11), 14178–14187.

(8) Storey, R. F.; Donnalley, A. B.; Maggio, T. L. Real-Time Monitoring of Carbocationic Polymerization of Isobutylene Using in Situ FTIR-ATR Spectroscopy with Conduit and Diamond-Composite Sensor Technology. *Macromolecules* **1998**, *31* (5), 1523–1526.

(9) Adamczyk, K.; Premont-Schwarz, M.; Pines, D.; Pines, E.; Nibbering, E. T. J. Real-Time Observation of Carbonic Acid Formation in Aqueous Solution. *Science* **2009**, *326* (5960), 1690–1694.

(10) Coblentz Society, Inc. Evaluated Infrared Reference Spectra. In *NIST Chemistry WebBook, NIST Standard Reference Database Number 69*; National Institute of Standards and Technology: Gaithersburg, MD 20899.

(11) Maher, R. C.; Cohen, L. F.; Gallop, J. C.; Le Ru, E. C.; Etchegoin, P. G. Temperature-Dependent Anti-Stokes/Stokes Ratios under Surface-Enhanced Raman Scattering Conditions. *J. Phys. Chem. B* **2006**, *110* (13), 6797–6803.

(12) Kinoshita, S.; Sakai, Y.; Miyazaki, J.; Watanabe, J. Fundamental Aspects of Light Scattering and Optical Kerr Effect Spectroscopy: From Basic Phenomena to Non-Quantum Behaviors. *Eur. Phys. J. Spec. Top.* **2012**, *209* (1), 1–100.

(13) Skoog, D. A.; Holler, F. J.; Crouch, S. R. Raman Spectroscopy. In *Principles of instrumental analysis*; Thomson Brooks/Cole: Belmont, CA, 2007; pp 481–497.

(14) Stiles, P. L.; Dieringer, J. A.; Shah, N. C.; Van Duyne, R. P. Surface-Enhanced Raman Spectroscopy. *Annu. Rev. Anal. Chem.* **2008**, *1* (1), 601–626.

(15) Morton, S. M.; Silverstein, D. W.; Jensen, L. Theoretical Studies of Plasmonics Using Electronic Structure Methods. *Chem. Rev.* **2011**, *111* (6), 3962–3994.

(16) Schatz, G. C.; Young, M. A.; Duyne, R. P. V. Electromagnetic Mechanism of SERS. *Appl. Phys.* **2006**, *103* (1), 19–46.

(17) Lyon, L. A.; Keating, C. D.; Fox, A. P.; Baker, B. E.; He, L.; Nicewarner, S. R.; Mulvaney, S. P.; Natan, M. J. Raman Spectroscopy. *Anal. Chem.* **1998**, *70* (1), 341–361.

(18) Kelly, K. L.; Coronado, E.; Zhao, L. L.; Schatz, G. C. The Optical Properties of Metal Nanoparticles: The Influence of Size, Shape, and Dielectric Environment. *J. Phys. Chem. B* **2003**, *107* (3), 668–677.

(19) Lombardi, J. R.; Birke, R. L.; Lu, T.; Xu, J. Charge-transfer Theory of Surface Enhanced Raman Spectroscopy: Herzberg–Teller Contributions. *J. Chem. Phys.* **1986**, *84* (8), 4174–4180.

(20) Xie, W.; Herrmann, C.; Kömpe, K.; Haase, M.; Schlücker, S. Synthesis of Bifunctional Au/Pt/Au Core/Shell Nanoraspberries for in Situ SERS Monitoring of Platinum-Catalyzed Reactions. *J. Am. Chem. Soc.* **2011**, *133* (48), 19302–19305.

(21) Shen, J.; Zhou, Y.; Huang, J.; Zhu, Y.; Zhu, J.; Yang, X.; Chen, W.; Yao, Y.; Qian, S.; Jiang, H.; Li, C. In-Situ SERS Monitoring of Reaction Catalyzed by Multifunctional Fe_3O_4@TiO_2@Ag-Au Microspheres. *Appl. Catal. B Environ.* **2017**, *205* (1), 11–18.

(22) Zheng, G.; Polavarapu, L.; Liz-Marzán, L. M.; Pastoriza-Santos, I.; Pérez-Juste, J. Gold Nanoparticle-Loaded Filter Paper: A Recyclable Dip-Catalyst for Real-Time Reaction Monitoring by Surface-Enhanced Raman Scattering. *Chem. Commun.* **2015**, *51* (22), 4572–4575.

(23) Deschaines, T. O.; Carron, K. T. Stability and Surface Uniformity of Selected Thiol-Coated SERS Surfaces. *Appl. Spectrosc.* **1997**, *51* (9), 1355–1359.

(24) Xie, W.; Walkenfort, B.; Schlücker, S. Label-Free SERS Monitoring of Chemical Reactions Catalyzed by Small Gold Nanoparticles Using 3D Plasmonic Superstructures. *J. Am. Chem. Soc.* **2013**, *135* (5), 1657–1660.

(25) Zhang, D. Decomposition of Rhodamine 6G in the Presence of Titania Coupling Coupled with Carbon Source as Photocatalyst under Visible Light Excitation. *High Energy Chem.* **2013**, *47* (4), 177–181.

(26) Nascimento, K. N. da S.; de Oliveira, M. C. A.; Oliveira, P. S.; Macedo, E. R.; de Oliveira, H. P. Photocatalytic Activity of ZnO Composites against Rhodamine B and Rhodamine 6G. *Fibers Polym.* **2015**, *16* (10), 2177–2183.

(27) Asiri, A. M.; Al-Amoudi, M. S.; Al-Talhi, T. A.; Al-Talhi, A. D. Photodegradation of Rhodamine 6G and Phenol Red by Nanosized TiO_2 under Solar Irradiation. *J. Saudi Chem. Soc.* **2011**, *15* (2), 121–128.

(28) Rasheed, T.; Bilal, M.; Iqbal, H. M. N.; Hu, H.; Zhang, X. Reaction Mechanism and Degradation Pathway of Rhodamine 6G by Photocatalytic Treatment. *Water. Air. Soil Pollut.* **2017**, *228* (291), 1–10.

(29) Wahab, R.; Khan, F. Statistical Parameters Effects on Photocatalytic Degradation of Rhodamine 6G Dye with Hexagonal Zinc Oxide Nanorods Synthesized via Solution Process. *J. Electron. Mater.* **2014**, *43* (11), 4266–4274.

(30) Luo, Y.; Li, K.; Wen, G.; Liu, Q.; Liang, A.; Jiang, Z. A Rapid Surface-Enhanced Raman Scattering Method for the Determination of Trace Hg^{2+} Using Rhodamine 6G-Aggregated Nanosilver as Probe. *Plasmonics* **2012**, *7* (3), 461–468.

(31) Su, S.; Zhang, C.; Yuwen, L.; Chao, J.; Zuo, X.; Liu, X.; Song, C.; Fan, C.; Wang, L. Creating SERS Hot Spots on MoS_2 Nanosheets with in Situ Grown Gold Nanoparticles. *ACS Appl. Mater. Interfaces* **2014**, *6* (21), 18735–18741.

(32) Watanabe, H.; Hayazawa, N.; Inouye, Y.; Kawata, S. DFT Vibrational Calculations of Rhodamine 6G Adsorbed on Silver: Analysis of Tip-Enhanced Raman Spectroscopy. *J. Phys. Chem. B* **2005**, *109* (11), 5012–5020.

(33) Kimling, J.; Maier, M.; Okenve, B.; Kotaidis, V.; Ballot, H.; Plech, A. Turkevich Method for Gold Nanoparticle Synthesis Revisited. *J. Phys. Chem. B* **2006**, *110* (32), 15700–15707.

(34) Liu, B.; Han, G.; Zhang, Z.; Liu, R.; Jiang, C.; Wang, S.; Han, M.-Y. Shell Thickness-Dependent Raman Enhancement for Rapid Identification and Detection of Pesticide Residues at Fruit Peels. *Anal. Chem.* **2012**, *84* (1), 255–261.

(35) Sackmann, M.; Materny, A. Surface Enhanced Raman Scattering (SERS)—a Quantitative Analytical Tool? *J. Raman Spectrosc.* **2006**, *37* (1–3), 305–310.

(36) Pamies, R.; Cifre, J. G. H.; Espín, V. F.; Collado-González, M.; Baños, F. G. D.; de la Torre, J. G. Aggregation Behaviour of Gold Nanoparticles in Saline Aqueous Media. *J. Nanoparticle Res.* **2014**, *16* (4), 1–11.

(37) Wallace, F. Expanding the Applicability of Raman Spectroscopy for Monitoring Photocatalytic Degradation. Honors College Capstone Experience, Western Kentucky University, Bowling Green, KY, 2016.

(38) Preininger, C.; Mohr, G. J.; Klimant, I.; Wolfbeis, O. S. Ammonia Fluorosensors Based on Reversible Lactonization of Polymer-Entrapped Rhodamine Dyes, and the Effects of Plasticizers. *Anal. Chim. Acta* **1996**, *334* (1–2), 113–123.

(39) Selwyn, J. E.; Steinfeld, J. I. Aggregation of Equilibriums of Xanthene Dyes. *J. Phys. Chem.* **1972**, *76* (5), 762–774.

(40) Arbeloa, F. L.; Gonzalez, I. L.; Ojeda, P. R.; Arbeloa, I. L. Aggregate Formation of Rhodamine 6G in Aqueous Solution. *J. Chem. Soc. Faraday Trans. 2* **1982**, *78* (7), 989–994.

(41) Valdes-Aguilera, O.; Neckers, D. C. Aggregation Phenomena in Xanthene Dyes. *Acc. Chem. Res.* **1989**, *22* (5), 171–177.

(42) Inaoka, W.; Harada, S.; Yasunaga, T. Kinetic and Spectrophotometric Studies of Rhodamine 6G Dimerization in Aqueous Solution. *Bull. Chem. Soc. Jpn.* **1980**, *53* (8), 2120–2122.

(43) Adachi, K.; Watanabe, K.; Yamazaki, S. PH-Responsive Switchable Aggregation Phenomena of Xanthene Dyes Adsorbed on Tungsten (VI) Oxide Colloid Surface. *Ind. Eng. Chem. Res.* **2014**, *53* (33), 13046–13057.